Acta Biomaterialia 176 (2024) 156–172

Contents lists available at ScienceDirect

Acta Biomaterialia

journal homepage: www.elsevier.com/locate/actbio

Full length article

Hybrid hydrogels support neural cell culture development under magnetic actuation at high frequency

Julia Martínez-Ramírez[1], Marta Toldos-Torres[1], Esther Benayas, Natalia Villar-Gómez, Laura Fernández-Méndez, Francisco M. Espinosa, Ricardo García, Sabino Veintemillas-Verdaguer, María del Puerto Morales, María Concepción Serrano*

Instituto de Ciencia de Materiales de Madrid, Consejo Superior de Investigaciones Científicas, Calle Sor Juana Inés de la Cruz 3, Madrid 28049, Spain

ARTICLE INFO

Article history:
Received 21 October 2023
Revised 8 January 2024
Accepted 22 January 2024
Available online 27 January 2024

Keywords:
Collagen
Iron oxide nanoparticles
Magnetic hydrogels
Primary neural cells
Neural repair

ABSTRACT

The combination of hydrogels and magnetic nanoparticles, scarcely explored to date, offers a wide range of possibilities for innovative therapies. Herein, we have designed hybrid 3D matrices integrating natural polymers, such as collagen, chitosan (CHI) and hyaluronic acid (HA), to provide soft and flexible 3D networks mimicking the extracellular matrix of natural tissues, and iron oxide nanoparticles (IONPs) that deliver localized heat when exposed to an alternating magnetic field (AMF). First, colloidally stable nanoparticles with a hydrodynamic radius of ~20 nm were synthesized and coated with either CHI (NPCHI) or HA (NPHA). Then, collagen hydrogels were homogeneously loaded with these coated-IONPs resulting in soft ($E_0 \sim 2.6$ kPa), biodegradable and magnetically responsive matrices. Polymer-coated IONPs in suspension preserved primary neural cell viability and neural differentiation even at the highest dose (0.1 mg Fe/mL), regardless of the coating, even boosting neuronal interconnectivity at lower doses. Magnetic hydrogels maintained high neural cell viability and sustained the formation of highly interconnected and differentiated neuronal networks. Interestingly, those hydrogels loaded with the highest dose of NPHA (0.25 mgFe/mg polymer) significantly impaired non-neuronal differentiation with respect to those with NPCHI. When evaluated under AMF, cell viability slightly diminished in comparison with control hydrogels magnetically stimulated, but not compared to their counterparts without stimulation. Neuronal differentiation under AMF was only affected on collagen hydrogels with the highest dose of NPHA, while non-neuronal differentiation regained control values. Taken together, NPCHI-loaded hydrogels displayed a superior performance, maybe benefited from their higher nanomechanical fluidity.

Statement of significance

Hydrogels and magnetic nanoparticles are undoubtedly useful biomaterials for biomedical applications. Nonetheless, the combination of both has been scarcely explored to date. In this study, we have designed hybrid 3D matrices integrating both components as promising magnetically responsive platforms for neural therapeutics. The resulting collagen scaffolds were soft ($E_0 \sim 2.6$ kPa) and biodegradable hydrogels with capacity to respond to external magnetic stimuli. Primary neural cells proved to grow on these substrates, preserving high viability and neuronal differentiation percentages even under the application of a high-frequency alternating magnetic field. Importantly, those hydrogels loaded with chitosan-coated iron oxide nanoparticles displayed a superior performance, likely related to their higher nanomechanical fluidity.

© 2024 The Author(s). Published by Elsevier Ltd on behalf of Acta Materialia Inc.
This is an open access article under the CC BY license (http://creativecommons.org/licenses/by/4.0/)

1. Introduction

Nanomedicine applied to neural tissue regeneration is a relatively new field rapidly expanding in which nanosystems are being used to administer therapeutic medicines to specific neural targets while monitoring/promoting local regenerative processes.

* Corresponding author.
E-mail address: mc.terradas@csic.es (M.C. Serrano).
[1] These authors contributed equally to this work.

https://doi.org/10.1016/j.actbio.2024.01.030
1742-7061/© 2024 The Author(s). Published by Elsevier Ltd on behalf of Acta Materialia Inc. This is an open access article under the CC BY license (http://creativecommons.org/licenses/by/4.0/)

However, nanomedicines are speedily uptaken and degraded by immune cells, shortening their lifetime and hampering their concentration in target tissues, further hindered by the blood-brain and blood-spinal cord barriers. One of the most attractive strategies to counteract these difficulties is their complexation into hybrid materials based on hydrogels, which are soft polymeric materials finely mimicking the extracellular matrix of native tissues through which cellular containment and guidance is provided [1]. As highly hydrated 3D structures widely explored in biomedicine [2–4], they show a notable capability for entrapping large quantities of solutes including drugs, signaling molecules and nanoparticles [5–7]. Within natural polymers, collagen is one of the most extensively explored to date [8–11], including neural targets such as the brain and the spinal cord [12]. As a main structural protein of the extracellular matrix, collagen possesses innate pro-regenerative properties [8] and is broadly available in nature, biocompatible, biodegradable, and easily recognized by cells [13,14].

An extensive variety of nanoparticles have been explored to date as nanocarriers for neural tissue engineering [15], including polymeric nanoparticles, quantum dots, and inorganic nanoparticles, among many others. For instance, multicomponent silica nanoparticles with an iron oxide core responding to low-power radiofrequency fields have been already explored for drug delivery applications in brain tumours [16]. Within biocompatible and biodegradable nanosystems, the incorporation of iron oxide nanoparticles (IONPs) into hydrogels is particularly attractive as it confers magnetic responsiveness for controlled movement in response to magnetic gradients and generates localized heat through magnetic hyperthermia. Additionally, if being superparamagnetic, IONPs are able to magnetically respond to an external magnetic field but lose their magnetization when the stimulus is removed [17]. Moreover, IONPs offer a scalable and inexpensive production in comparison to other nanomaterials [18,19]. Regarding their application, IONPs have been mostly used as contrast agents for magnetic resonance imaging (MRI) and drug delivery systems for cancer treatment [20,21], having attained FDA approval (*e.g.,* Ferumoxytol [22] and NanoTherm® [23]) and reached clinical trials (contrast agents: NCT00920023, NCT01927887, NCT04803331, and NCT05359783; cancer: NCT04682847 and NCT04316091). Importantly, their theranostic application enormously depends on their physico-chemical characteristics, such as particle size, shape, surface area and charge, colloidal stability, and magnetic properties [24].

Most magnetically responsive hydrogels have been applied in drug delivery, magnetic hyperthermia, artificial muscles, and cell activation [25,26], but being rarely explored to date for neural regeneration even being those electrically active tissues prompt to respond to magnetic and electrical stimuli. Some examples of their use in drug delivery include the release of sunitinib [27], levodopa [28] and doxorubicin [29], with a significant improvement in therapeutic efficacy in tumour-bearing mice. In the context of neural regeneration, they have been mainly explored for driving neuronal orientation [30–32] and controlling topographical and biochemical cues [33,34]. When embedded in hydrogels, IONPs serve the preparation of ordered and gradient scaffolds with superior internal complexity and versatility able to govern cell behaviour including migration, direction and differentiation, and thereby guiding tissue regeneration [35]. Moreover, the confinement of the heat generated under magnetic stimulation in the IONP close vicinity is expected to help controlling both scaffold degradation and drug delivery by remote actuation.

From a therapeutical point of view, the possibility to remotely control intracellular pathways using magnetic fields offers the option to manipulate biological processes with spatial and temporal resolution, although there are still many obstacles to overcome prior to make this a real clinical alternative [36]. In this work, we have designed novel magnetically responsive hydrogels by embedding IONPs prepared by co-precipitation in highly porous collagen matrices fabricated by freeze-casting. In order to augment IONP colloidal stability and interaction within the collagen matrix, two biocompatible polymers with attractive properties for tissue regeneration, chitosan and hyaluronic acid, were selected to coat IONPs and their impact in the response of primary neural cells carefully investigated and compared. The alkaline polysaccharide chitosan (CHI) is universally available at low cost, fully bioresorbable, free of toxic metabolites eventually interfering regeneration and neuroprotector [37–39]. CHI-coated IONPs have been mainly used as nanocarriers for antitumoral drugs [40–42] and cell tracking by MRI based on their superior cell internalization [43,44], being already tested for labelling embryonic mouse neural stem cells, among others. Alternatively, hyaluronic acid (HA) is a linear, non-branched, negatively charged heteropolysaccharide [45–47]. HA can bind up to 1,000 times more water molecules than the weight of the macromolecule itself, adopting an enlarged conformation and forming gels even at very low concentrations [46,47]. HA molecules elicit receptor-mediated signalling pathways in cells depending on their concentration and molecular weight (Mw). As for CHI, HA has been used for cancer drug delivery and MRI. As known to be preferentially internalized by $CD44^+$ cells [48,49], HA-coated IONPs have been already explored for cisplatin and paclitaxel delivery in cancer cells [50,51]. In the context of neural regeneration, HA hydrogels have been explored for brain repair after stroke [52].

After a careful characterization of the physico-chemical properties of the materials developed, the biological responses of primary neural cells isolated from E17 rat cerebral cortices exposed to both, polymer-coated IONPs and magnetic hydrogels, were tested *in vitro* with and without magnetic stimulation, separately and in combination. For all conditions, major parameters under investigation included viability, morphology, scaffold colonization, and neural differentiation.

2. Experimental section

2.1. Material

All reagents were commercially purchased and used as received, unless otherwise indicated. $FeCl_2{\cdot}4H_2O$ (≥ 99.0%, Sigma-Aldrich), $FeCl_3$ aq. (27 % wt, Sigma-Aldrich), NH_4OH (25 %, Sigma-Aldrich), HNO_3 (< 65 %, Sigma-Aldrich), and $Fe(NO_3)_3{\cdot}9H_2O$ (> 98.0%, Sigma-Aldrich) were used. Lyophilized CHI powder from shrimp shells (>75% deacetylated, reference C3646), HA powder (low viscosity, low endotoxin, reference 924474) and collagen solution from bovine skin (3 mg/mL, reference C4243) were acquired from Merck. Antibodies were bought from Sigma-Aldrich and Invitrogen. Neurobasal™ media, B-27 supplement and GlutaMAX® were purchased from ThermoFisher. All materials and biological samples in this study were handled according to standard regulations to prevent safety concerns.

2.2. IONP fabrication

Magnetic IONPs were synthesized by Massart's co-precipitation protocol [53]. Briefly, 75 mL of NH_4OH (25 %) were quickly added to a mixture of 445 mL of $FeCl_3{\cdot}6H_2O$ (0.09 mol) and $FeCl_2{\cdot}4H_2O$ (0.054 mol). The resulting sample was washed three times by magnetic decantation with distilled water. To improve the colloidal properties and stability of the sample [54], the precipitate was treated with 300 mL of HNO_3 (2M) under stirring for 15 min. HNO_3 was then removed, by magnetic decantation, and 75 mL of $Fe(NO_3)_3$ (1M) with 130 mL of distilled water were added. The mixture was brought to 90 ºC for 30 min and cooled down to room temperature. As before, the supernatant was exchanged with 300

mL of HNO_3 (2M) under stirring for 15 min. Finally, IONPs were washed three times with distilled water.

2.3. IONPs surface coating and characterization

For IONP coating with CHI, a polymer solution was prepared by dissolving CHI powder (1 mg/mL) in acetic acid (10 mM) overnight. After mixing IONPs and CHI during 15 min in sonication, sodium tripolyphosphate (TPP; Sigma-Aldrich), acting as a crosslinker, was added to the suspension drop by drop. The suspension was left for another 30 min in sonication. Several IONPs:polymer weight ratios were tested (1:2, 2:1, 5:1, 10:1, 20:1, 30:1, and 50:1). For ratios smaller than 10:1, the hydrodynamic radius of the nanoparticles obtained ranged from 100-500 nm, too large for the purposes pursued in this work. On the contrary, a 30:1 ratio generated nanoparticles under 100 nm in size and was used throughout this work. The amount of TPP selected in this work (18:1 ratio, IONPs:TPP) was reduced in comparison to that reported in previous work [55] to preserve the hydrodynamic size below 100 nm. The resulting coated-IONP suspension (NPCHI) was washed two times with distilled water and stored at 4°C until use. The deacetylation degree (DA) of CHI was determined as previously described by Muzzarelli and Rochetti [56] and its M_w and averaged molecular weight (M_n) was measured using a size exclusion-high-performance liquid chromatography operated in a Waters 625 LC System pump with an Ultrahydrogel column at 35 ºC and a Waters 2414 differential refractometer (Milford, MA, USA). Ammonium acetate/acetic acid buffer (pH = 4.5) was used as eluent (flow rate of 0.6 mL/min). Specifically, the chitosan used in this study presented a M_w of 17,373 kDa, a M_n of 127 kDa (PDI = 13.7), and a DA degree of 81.4 %. These data indicate that our polymer solution contained a broad M_w distribution, with a clear majority of chains being deacetylated and having high M_w. It has been reported that higher DA values decrease CHI biodegradation rate, while high M_w reduces polymer fluidity, both aspects being pivotal when controlling tissue interactions [37]. The CHI used in this study presented high M_w and DA degree, selected because of its anti-apoptotic effects and better adhesion and growth of neural cells associated [57–59].

For IONPs coating with HA, the same procedure as for CHI was followed to reach the optimum IONPs-polymer ratio, corroborating that a 30:1 ratio yielded the smallest hydrodynamic sizes. HA was dissolved (1 mg/mL) in distilled water by mild magnetic stirring at room temperature for 15 min. Then, IONPs were added and left for 15 min under sonication. The resulting polymer-coated IONPs suspension (NPHA) was stored at 4°C until use.

Particle size of non-functionalized IONPs was determined using a 200 keV JOL-2000FXII transmission electron microscope (TEM). A diluted drop of the aqueous IONP suspension was placed on a carbon-coated copper grid. More than 150 nanoparticles were measured from TEM images by using the software ImageJ and adjusting the obtained data to a lognormal distribution. Colloidal properties for all samples were characterized by dynamic light scattering (DLS) using a Zetasizer instrument (Malvern). Z-average values in number at pH = 5 were used as the mean hydrodynamic size and the Z potential was measured in a KNO_3 solution (0.01 M) at the same pH. Either HNO_3 or KOH was added to the solution to vary the pH value. The Fe concentration in IONP colloids and cell suspensions (5×10^5 cells) was determined by inductively coupled plasma optical emission spectroscopy (ICP-OES) in a PERKIN ELMER OPTIMA 2100 DV apparatus after digestion with aqua regia at 90 ºC (total volume of 10 mL). In the case of cell suspensions, concentrations selected for both NPCHI and NPHA were the highest (0.1 mg Fe/mL) and the lowest (0.001 mg Fe/mL) ones at 2 h and 24 h.

For powder-based physico-chemical characterization, IONPs suspensions were lyophilized at -70°C and 0.2 mbar for 2 days. X-ray diffraction (XRD) patterns were collected on powder samples using a D8 Advance A25 instrument (Bruker) with CuKα1 radiation (λ = 1.5406 Å) and a PSD-XE detector (DAVINCI). XRD patterns were obtained from 2θ = 20° - 70° in steps of 0.03° and time steps of 2 s. For Fourier transform infrared (FTIR) studies, IONPs were diluted in KBr at 2 % and pressed in pellets. FTIR spectra were acquired between 4000 and 250 cm^{-1} by using a Vertex 70V FTIR (Bruker) to confirm the ferrite phase and the presence and nature of the coating. Thermogravimetry analysis (TGA) was performed in a Seiko, TG/DTA EXSTAR 6000 thermobalance by heating the samples under 100 mL/min air flow from 25° to 900° at 5° min^{-1}. Magnetic characterization was performed using a vibrating sample magnetometer (VSM), operating in the 5-300 K temperature range (maximum applied field 50 kOe) in dried powder samples. The magnetic heating capacity of the IONP aqueous suspensions was measured by a Five Celes AC magnetic field inductor equipped with a water cooled 50 mm diameter coil of 6 turns. The temperature was registered with an optic fibre thermal probe (OSENSA). The specific absorption rate (SAR) was then calculated for each sample as previously reported [60].

2.4. Fabrication and characterization of magnetic hydrogels

For collagen hydrogels loaded with NPCHI (HG/NPCHI), the mass NPCHI/polymer ratios ranged between ~0.1 (low) and 1.1 (high). In the case of collagen hydrogels containing NPHA (HG/NPHA), the mass NPHA/polymer ratios ranged between ~0.05 (low) and 0.5 (high). The different concentration ranges employed in both cases were due to previous toxicity results of the coated IONPs in primary neural cells. For the preparation of each hydrogel, 100 µL of the solution of collagen with IONPs were pipetted into the cap of 0.5 mL eppendorf tubes, immediately frozen at -80 °C for 5-6 h and later lyophilized for 48 h to obtain randomly porous 3D scaffolds. The resulting scaffolds were then crosslinked by exposure to 4 % paraformaldehyde (PFA) vapors for 2 h under stirring.

For morphological characterization of the resulting hydrogels, a Hitachi S–3000 N, a last generation ultrahigh resolution FEI VERIOS 460 and a JEM1400 Flash (Jeol) electron microscopes were employed. Fiber diameter and pore size were measured from these micrographs by using the ImageJ software. FTIR spectra were acquired as described for IONPs to confirm the nature of the polymer and its specific chemical interactions with IONPs. For these studies, hydrogel samples were diluted in KBr at 2 % and pressed in pellets. TGA studies were performed as for IONP characterization. To analyze swelling capacity, hydrogels were weighted before and after immersion in distilled water for 24 h of hydration to measure the mass change. Swelling rates at different times were calculated as $(W_s\text{-}W_d)/W_d$, where W_s is the weight of hydrogels in the swollen state and W_d is their initial weight in the dry state. *In vitro* degradation of the hydrogels was studied for up to 3 months in distilled water at room temperature. The gross morphology of the hydrogels was monitored weekly by using a magnifying glass (Leica). AFM nanoindentation experiments were performed with a borosilicate glass probe (10 µm of diameter). The cantilever constant was 0.08 N/m (nominal value). The force-distance curves were acquired at a constant velocity of 10 µm/s. The probe indented the hydrogel until a peak force of 10 nN was measured. The curves were measured on 20 different locations of the surface (10 curves on each point). The measurements were performed in phosphate buffered saline (PBS). AFM nanoindentation data were analyzed in terms of the power-law rheology model as previously described [61]. Finally, the magnetic properties of the resulting hydrogels were studied by using a

VSM, operating with the same parameters as for IONPs magnetic characterization.

2.5. Primary neural cell isolation, culture and IONP exposure

Embryonic neural progenitor cells (ENPCs) were isolated from cerebral cortices of E17 rat embryos as previously established in our laboratory [62,63]. All the experimental protocols for cell collection adhered to the regulations of the European Commission (directives 2010/63/EU and 86/609/EEC) and the Spanish Government (RD53/2013 and ECC/566/2015) for the protection of animals used for scientific purposes. Adult female Wistar rats were provided by the animal facilities of the National Hospital for Paraplegics (Toledo) and sacrificed by CO_2 inhalation when gestation reached 17 days. Six independent cell cultures were carried out ($N \geq 3$ for each parameter under investigation and duplicates per culture condition), with cell viability above 80 % in all cases. Prior to cell culture, polymer-coated IONP suspensions were filtered through 0.4 μm filters and crosslinked hydrogels were sterilized under UV radiation for 30 min in a safety cabinet. Both glass coverslips (12 mm in diameter) and magnetic hydrogels were coated with poly($_L$-lysine) (PLL) (45 µg mL^{-1} in borate buffer 0.1 M, pH = 8.4) for 1 h at room temperature, carefully washed with borate buffer and then conditioned for 2 h in complete culture medium in a sterile incubator at 37 °C under a CO_2 atmosphere (5%).

For IONP biocompatibility assays, cell seeding density was 25×10^3 cells/cm^2. Cells were maintained in complete Neurobasal™ medium containing B-27 supplement (2 %), streptomycin (100 UI/mL), penicillin (100 UI/mL), and GlutaMAX® (1 %), in a sterile incubator at 37 °C under a CO_2 atmosphere (5%). Culture media were half-replaced every 3-4 days. After 7 days *in vitro* (DIV), cells were exposed to five different doses of polymer-coated IONPs (0.001, 0.005, 0.01, 0.05, and 0.1 mg Fe/mL) for 24 h. After IONP exposure, cultures were gently washed with warm sterile PBS and culture media was replaced, leaving the cells for another 24 h of recovery before examination.

For magnetic hydrogel biocompatibility assays, ENPCs were directly seeded on PLL-coated hydrogels at a density of 500 000 cells/hydrogel and cultures were maintained for 14 DIV in complete Neurobasal™ medium, being also half replaced every 3–4 days. ENPC culture evolution was monitored during culture at the periphery of the hydrogels by using an Axiovert CFL-40 optical microscope with a coupled Axiocam ICC-1 digital camera (Zeiss), confirming that neither the components/leachables of these magnetic hydrogels nor PFA exposure were toxic for these primary neural cells.

2.6. Cell culture morphology and IONP internalization assays

ENPC cultures exposed to either IONPs or corresponding magnetic hydrogels were fixed with glutaraldehyde (2.5 % in distilled water) for 45 min at room temperature and dehydrated in series of ethanol with increasing concentrations (30, 50, 70, 90 and 100 %) for 15 min each (twice). Once completely dried, samples were mounted on metal stubs using carbon tape. Finally, samples were coated with a thin chromium layer and visualized by using a FEI VERIOS 460 scanning electron microscope (SEM). To further investigate the eventual internalization of polymer-coated IONPs by neural cells, ENPCs were incubated with IONPs at 0.1 mg Fe/mL for 24 h and fixed with glutaraldehyde and osmium tetroxide. Then, samples were dehydrated, embedded in epoxy resin for ultrathin sectioning and finally observed by using a 200 keV JEOL-2000FXII transmission electron microscope (TEM).

2.7. Viability assays

Cell viability was evaluated by using a Live/Dead® kit according to the manufacturer's instructions (Invitrogen). This kit is based on calcein (live cells emitting intense green fluorescence) and ethidium homodimer-1 (EthD-1; dead cells emitting intense red fluorescence). After incubation with the probes for 5 min at 37 ºC, samples were visualized with a Leica SP5 confocal laser scanning microscope (CLSM). The fluorescence of both probes was excited by an argon laser tuned to 488 nm. After excitation, emitted fluorescence was separated using a triple dichroic filter 488/561/633 and measured in the range of 505-570 nm for green fluorescence (calcein) and 630-750 nm for red fluorescence (EthD-1). ImageJ software was employed to quantify cell viability by measuring both the area covered by green and red labelled cells as well as their numbers, which were expressed as a percentage of the total image area.

2.8. Neural differentiation assays

Cultured samples were fixed with paraformaldehyde (4% in PBS) for 15 min at room temperature, permeabilized with saponin and incubated with primary antibodies as follows: anti-MAP-2 and anti-β-III tubulin for labelling neurons, anti-vimentin for tagging non-neuronal cells including glial cells, and anti-synaptophysin for visualizing synapses in neurons. The secondary antibodies used were Alexa Fluor® 488 anti-mouse in goat IgG (H + L) and Alexa Fluor® 594 anti-rabbit in goat IgG (H + L). Cell nuclei were stained in blue with Hoechst. After staining, samples were visualized under a SP5 CLSM. Fluorochromes were excited and measured as follows: Alexa Fluor® 488 excitation at 488 nm with an argon laser and detection at 507-576 nm, Alexa Fluor® 594 excitation at 594 nm with a helium-neon laser and detection at 625-689 nm and Hoechst excitation at 405 nm with a diode UV laser and detection at 423-476 nm. To quantify cell differentiation, the green and red positive areas were measured by using the ImageJ software and normalized by their corresponding blue area.

2.9. Magnetic stimulation assays

For magnetic stimulation studies, ENPCs cultured on petri dishes of 3.5 cm in diameter (glass bottom for posterior visualization) were first treated with IONPs for 24 h. Cultures were then exposed to an AMF (H = 21.2 mT, f = 281 kHz, 1 h) applied by using a Five Celes 12118M01 apparatus. This device results from the combination of a frequency generator 100-400 kHz CELES MP 6 kW and a chilled coil 71 mm i.d. DT25901A. The system is capable of producing alternating magnetic fields up to 65 mT at 90 kHz. Higher frequencies could be obtained at the cost of decreasing the magnetic field intensity. ENPCs seeded on magnetic hydrogels for 14 DIV were exposed to similar AMF conditions. The temperature of the samples was maintained at 37 ºC throughout the experiments by using a thermostat and controlled by a sensitive (0.01 ºC) fiber optic infrared thermometer. After AMF stimulation, viability and neural differentiation were analysed in these samples as previously described in 2.7 and 2.8 sections.

2.10. Statistical analyses

Values are expressed as the mean ± standard error of at least 3 independent experiments ($N \geq 3$). In each experiment, samples were typically analysed in duplicate, with at least 3 images per replicate. Statistical analysis was performed by using the Statistical Package for the Social Sciences (SPSS, version 27.0, IBM). Comparisons among groups were done by one-way analysis of

variance (ANOVA) followed by either *post-hoc* Scheffé or Games-Howell tests (homogeneous *vs.* heterogeneous variances, respectively, as dictated by Levene's test). In all cases, the significance level was defined as $p < 0.05$.

3. Results and discussion

3.1. Characterization of polymer-coated IONPs

The nanoparticles used in this work consisted of uniform single core iron oxide further coated with either CHI or HA, resulting in two distinct types of nanoparticles: NPCHI and NPHA, respectively. Fig. 1 summarizes the main physicochemical characteristics of IONPs before and after coating. First, TEM micrographs showed that the spherical morphology and size of the iron oxide core were maintained after coating (Figs. 1A and S1A, B). This was also confirmed in XRD spectra (Fig. 1B), which revealed diffraction peaks in all cases, assigned to a spinel crystal structure (S.G. *Fd3m*) corresponding to either magnetite or maghemite. Its crystallite size was found around 9 nm, in agreement with the IONP core size obtained by TEM. Infrared spectra (Fig. 1C) exhibited common bands around 400, 600 and 3400 cm^{-1} that correspond, respectively, to the vibration of Fe-O bonds of the iron oxide core and to OH groups, present in the coatings and water molecules absorbed. The absorption band around 2890 cm^{-1}, clearly observed for polymer samples used as reference, is attributed to C-H bonds, typical of polysaccharides (*e.g.,* glucans, xylan) [64,65]. Bands at 1653, 1564 and 1325 cm^{-1} correspond to amide groups and those around 1150 - 1070 cm^{-1} are assigned to C-C and C-O-C bonds, present in both polymers. Whereas some of these bands appear overlapped by nitrate residues in coated IONPs, bands around 1150 - 1070 cm^{-1} served to confirm the presence of the polymer coatings on the IONPs [65]. Fig. 1D shows TGA and ATD results for both types of coated-IONPs – there is an important decrease in weight due to the physically adsorbed water (< 100 ºC), slightly superior for HA as expected from its higher water adsorption capacity, followed by the burning of the polymer coating at around 138 ºC for CHI (103 - 329 ºC) and around 166 ºC for HA (91 - 304 ºC). The weight loss of the second process is used to estimate the presence of 8 wt% of CHI and 7 wt% of HA coating.

Fig. 1E presents the hydrodynamic size distribution in number for bare and coated IONPs. Hydrodynamic sizes at pH = 5 were 23 and 38 nm for NPCHI and NPHA, respectively, slightly larger than the size of bare nanoparticles (15 nm). Nanoparticle size distribution in intensity revealed the existence of some NPHA with larger sizes (Fig. S1C; *ca.* 150 and 300 nm), not visualized in the size distribution by number due to their almost negligible representation in the sample. Regarding superficial charge, the isoelectric point of both types of IONPs showed a comparable behaviour at different pH values (Fig. S1D), being positively charged at pH below 6 and negatively charged above 8. However, around neutral pH values, although both IONPs displayed a negative surface charge, it was markedly more negative for NPCHI than NPHA and bare nanoparticles (Fig. 1F). This effect might be due to the contribution of TPP during coating, as revealed by the positive surface charge of NPCHI at this pH in the absence of TPP (Fig. S1D). This negative charge was more dramatically neutralized for NPCHI than NPHA after immersion in culture media, maybe due to a larger adsorption of proteins or nanoparticle aggregation. The fact that the HA coating results in a larger hydrodynamic size and more colloidally stable IONPs is related to a superior capacity of this polymer to form hydrophobic interactions and inter-molecular H-bonds among chains [47], providing steric stabilization.

Regarding magnetic properties, both types of IONPs exhibited similar *Ms* values (~60 emu/g) and superparamagnetic behaviour at room temperature (zero remanence magnetization and coercivity) (Fig. 1G), attributed to their single iron oxide core. The polymer coating did not seem to have any relevant impact on these properties, which showed typical S-shaped cycles without hysteresis. However, their heating capacity decreased in both samples, probably due to the shielding effect of the coating also responsible for the increase in the hydrodynamic size with respect to uncoated (bare) IONPs in distilled water (Fig. S1E). The fact that NPCHI displayed higher SAR values than NPHA in spite of the similar amount of polymer coating might be related to the different nature of both polymers, being the more rigid CHI more capable of transporting the heat than the soft HA chains. When characterized in complete Neurobasal™ medium instead of distilled water, both samples presented higher hydrodynamic sizes (> 500 nm) and smaller SAR values as a consequence of certain degree of nanoparticle aggregation and the increase of the shielding effect. These changes due to the formation of the protein corona, likely modulate the physicochemical properties of the IONPs affecting their stability [66]. For instance, Rampino *et al.* showed that loading different proteins into chitosan nanoparticles influenced changes in their size and surface charge, leading to their precipitation [67]. It is important to note that cell culture media did not heat under the AMF, meaning all registered heat came from the IONPs.

3.2. Biological responses of primary neural cells to polymer-coated IONPs

Primary neural cells extracted from E17 rat embryonic cerebral cortices were first isolated and characterized by flow cytometry to define their phenotype at the moment of seeding (Fig. S2). At this point, most of the cells were positive for βIII-tubulin (96.7 %), a high percentage was positive for vimentin (77.6 %), some others for MAP-2 (30.1 %), and a smaller amount for GFAP (7.5 %). These results were highly reproducible and have been confirmed to vary as a function of the age of the embryos used. Next, the so isolated cells were cultured in the presence of NPCHI and NPHA at different doses. ENPC cultures exposed to polymer-coated IONPs were first analysed by SEM for morphological characterization (Figs. 2A and S3A), displaying akin morphologies to those of control cells. The presence of NPCHI and NPHA tightly interacting with cell somas and neurites was clearly evident in both cases. By using TEM, we next investigated if NPCHI and NPHA were being internalized by ENPCs (Fig. 2A). We found both NPCHI and NPHA being engulfed by cells and inside intracellular vesicles, as confirmed by dark field acquisition, which illustrated IONPs as much brighter elements (Fig. S3B). Further ICP-OES measurements corroborated IONP uptake, being dependent on nanoparticle concentration, coating and cell exposure time. Specifically, we observed a superior cell uptake for NPCHI than NPHA (Table 1) in almost all the conditions tested (2 and 24 h of exposure; 0.001 and 0.1 mg Fe/mL), except for the highest IONP concentration at the longest time (0.1 mg Fe/mL after 24 h) in which NPCHI and NPHA seemed alike, maybe related to an uptake saturation for both IONPs already reached by NPCHI at 0.1 mg Fe/mL after 2 h. The superior cell internalization for NPCHI might be favoured by the presence of local positive charges provided by CHI, as suggested by others [44,68], which itself mediates a different interaction with proteins in culture me-

Table 1
Uptake of polymer-coated IONPs by ENPCs measured by ICP-OES.

IONP	Dose (mg Fe/mL)	2 h (pg Fe/cell)	24 h (pg Fe/cell)
NPCHI	0.001	9	33
	0.1	512	482
NPHA	0.001	0.0	0.2
	0.1	175	490

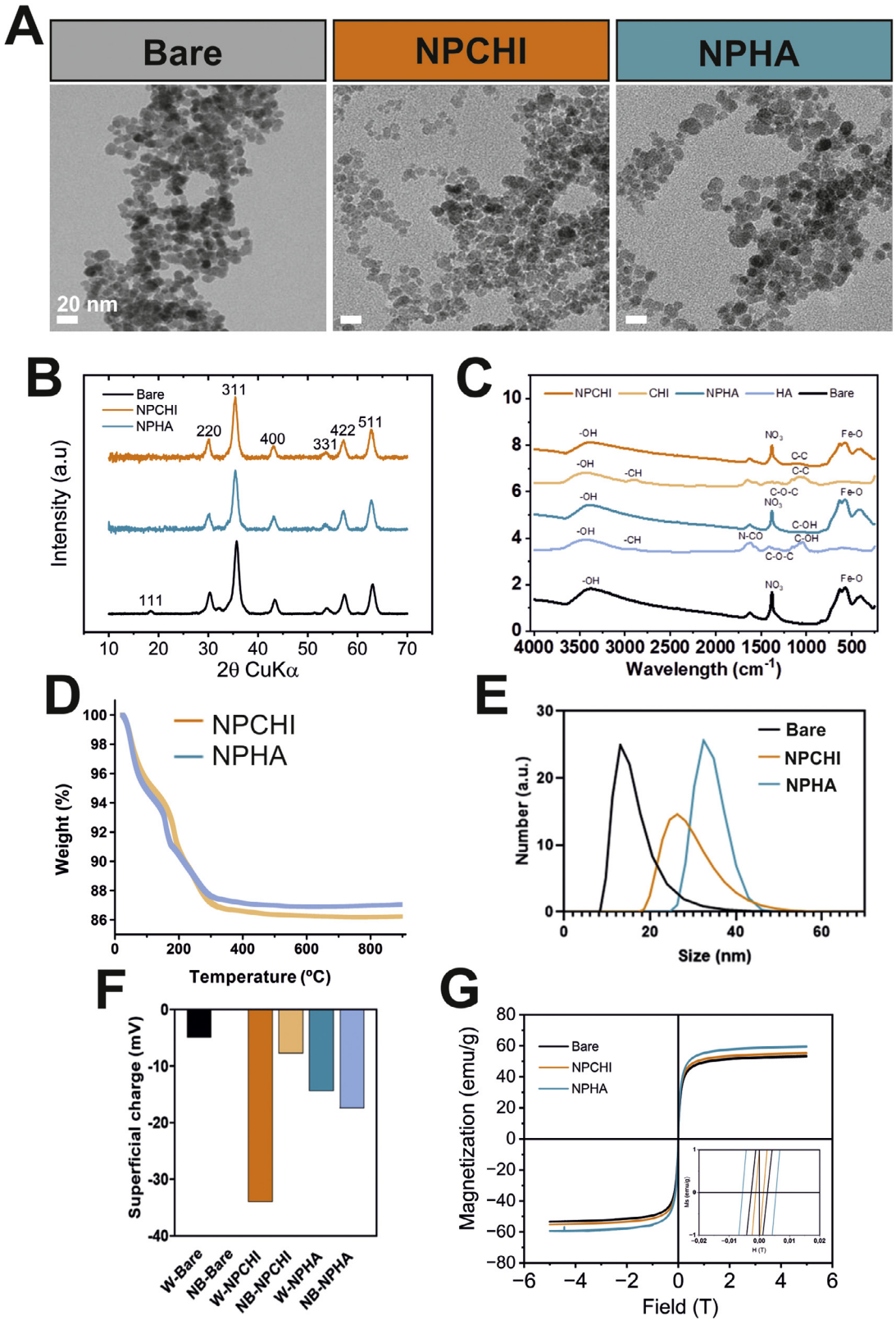

Fig. 1. Physicochemical characterization of polymer-coated IONPs. Representative TEM micrographs (A), XRD spectra (B), FTIR spectra (C), TGA (D), hydrodynamic size distribution in number at pH = 5 (E), superficial charge in distilled water (W) and neurobasal culture media (NB) (F) at pH = 8, and magnetic response (G) of bare IONPs (uncoated; gray-black), CHI-coated IONPs (NPCHI; orange) and HA-coated IONPs (NPHA; blue). Scale bars for TEM images: 20 nm.

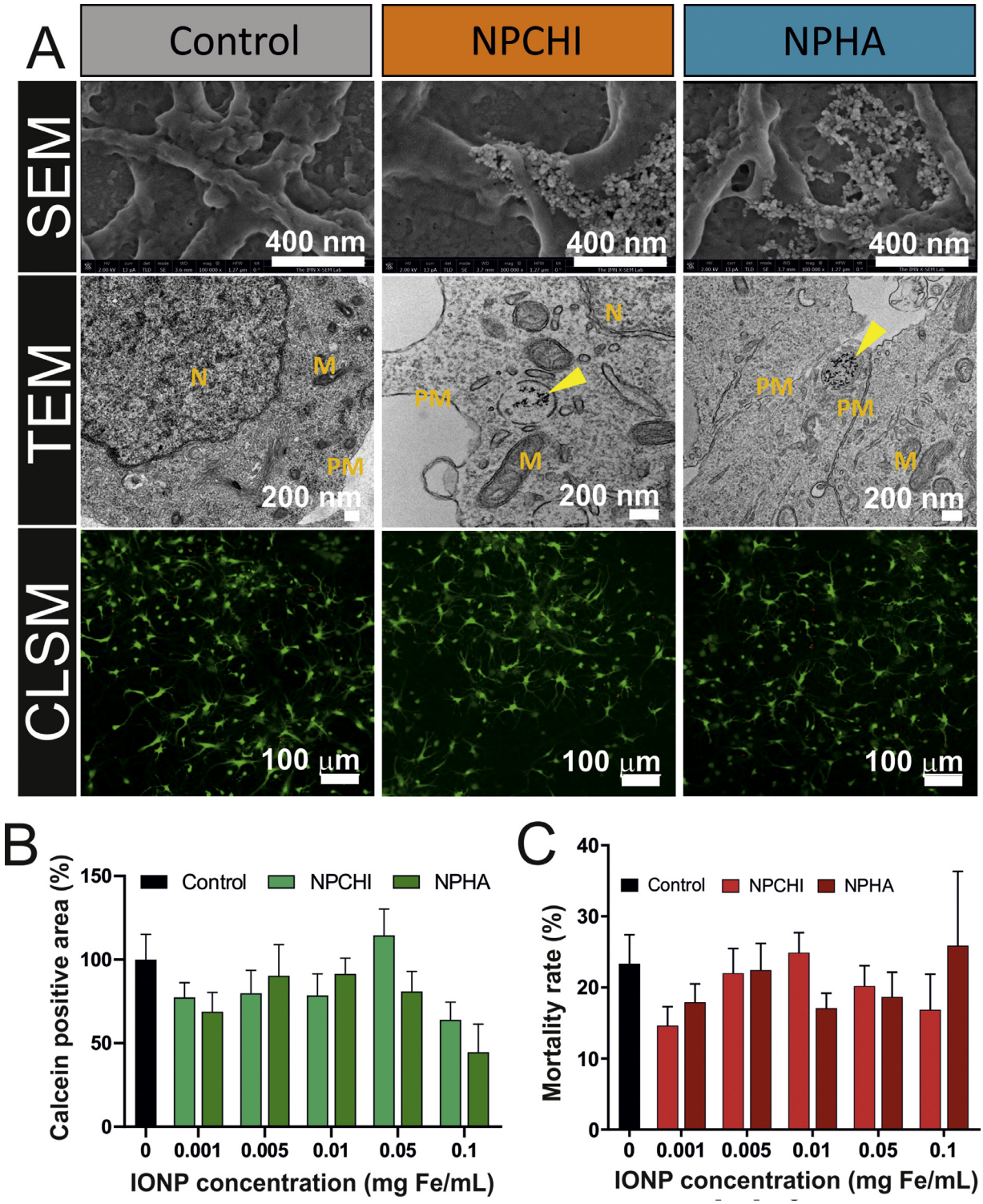

Fig. 2. Biological responses of ENPC cultures exposed to polymer-coated IONPs. (A) Representative SEM (top) and TEM (middle) images of cultures exposed to NPCHI and NPHA at 0.01 mg Fe/mL. In TEM micrographs, IONPs (yellow arrowheads), nucleus (N), plasma membrane (PM) and mitochondria (M) are indicated. Representative CLSM images (bottom) and respective quantitative data for cell viability measured as the positive area labelled with calcein (green fluorescence, live cells; B) and the number of cells stained by EthD-1 (red fluorescence, dead cells; C) for the different conditions tested. Scale bars: 400 nm (SEM), 200 nm (TEM) and 100 μm (CLSM). Statistics: one-way ANOVA followed by Scheffé *post hoc* test; N $\geq$ 3 experiments with duplicates per condition, n $\geq$ 3 images per replicate.

dia, first, and cell membranes later. In agreement with these findings, we have recently found a strong correlation between surface charge and cell uptake, even for IONPs with the same type of coating [69].

We then examined neural cell viability (Fig. 2A–C). There were not statistically significant differences in the area covered by live cells (ANOVA, $p > 0.05$ in all cases), even for the highest concentration tested (0.1 mg Fe/mL), thus revealing high viability with independence of the polymer coating. Nonetheless, this high concentration showed a detectable trend of decrease in viability for both IONPs, being larger for NPHA. In line with these results, there were not significant differences in cell death (expressed as the number of EthD-1-labelled cells normalized by the total number of cells in percentage) at any condition tested. Preliminary studies including bare IONPs showed higher cell mortality at all concentrations tested, even at 0.001 mg Fe/mL (Fig. S4), hence IONP coating was mandatory prior to any biological use of these IONPs.

Next, we investigated the effect of these polymer-coated IONPs on neural cell differentiation (Figs. 3, S5 and S6). Neurons were first identified by MAP-2 labelling and non-neuronal cells including glial cells by vimentin (Fig. 3A, top). No significant differences were found for any of the conditions tested (Fig. 3B, C), being all the cultures formed by both neurons, markedly more abundant, and non-neuronal cells including glial cells. The highest concentration of NPCHI showed a trend of decrease in non-neuronal cells. However, it is important to note that the amount of non-neuronal cells was more heterogeneous among experiments than that of neuronal cells, as evidenced by larger error bars, which made difficult to evidence significant differences among treatments. For a further examination of the differentiation process, neurons were identified by βIII-tubulin labelling and synaptic vesicles by synaptophysin (Fig. 3A, bottom). In agreement with MAP-2 results, neuronal differentiation was maintained in all groups (Fig. 3D). Regarding synapses (Fig. 3E), the amount of synaptophysin labelling was found very alike among conditions. The degree of architectural connectivity of the cultures was then evaluated by measuring the percentage of intersections of βIII-tubulin-labelled neurites (Fig. 3F). Interestingly, both NPCHI and NPHA reached and even surpassed values of control cultures. The enhancement in interconnectivity found for the lowest concentrations of NPHA (ANOVA followed by Scheffé *post hoc* test; 0.001 mg Fe/mL *vs* control: $p = 0.012^*$) and intermediate concentrations of NPCHI (ANOVA followed by Scheffé *post hoc* test; 0.005 mg Fe/mL *vs* control: $p = 0.039^*$) was especially relevant. Again, the highest concentrations of NPHA reversed such favourable finding (ANOVA followed by Scheffé *post hoc* test; 0.1 mg Fe/mL *vs* 0.001 mg Fe/mL: $p = 0.015^*$). Taken together, both kinds of nanoparticles not only maintained but even favoured the development of

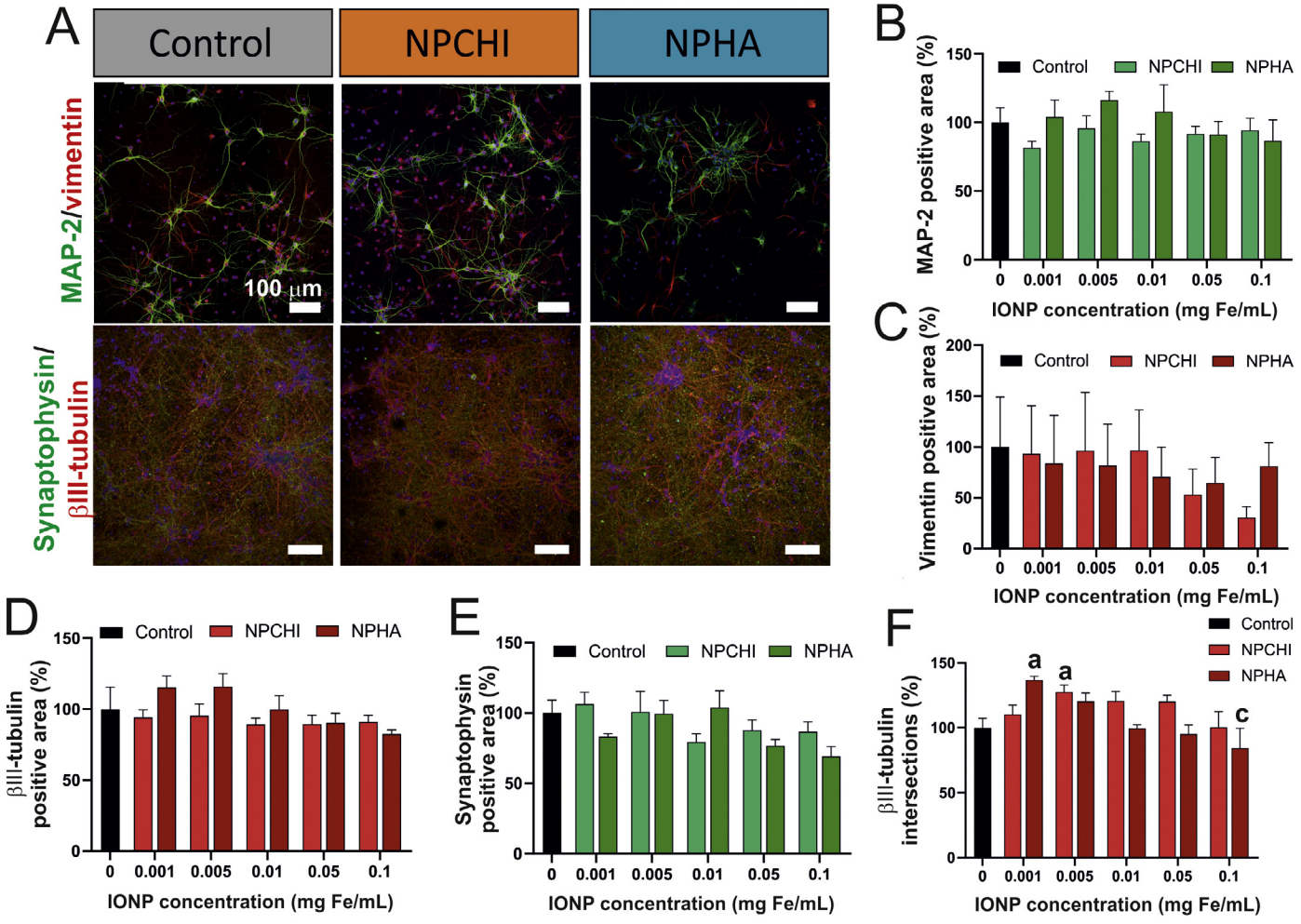

Fig. 3. Impact of polymer-coated IONPs on neural differentiation. Representative CLSM images of cultures exposed to NPCHI and NPHA at 0.01 mg Fe/mL for different markers as indicated (A). Cell nuclei appear in blue in all images (Hoechst). Scale bars: 100 μm in all images. Respective quantitative data of the positive area for MAP-2 (B), vimentin (C), βIII-tubulin (D), and synaptophysin (E). Number of intersections for βIII-tubulin$^+$ neurites (F). All values have been normalized by cell density (Hoechst staining). Statistics: one-way ANOVA followed by Scheffé *post hoc* test (as dictated by Levene's test); $N \geq 3$ experiments with duplicates per condition, $n \geq 3$ images per replicate. Significance: $p < 0.05$; comparisons with respect to control (a) and NPHA 0.001 mg Fe/mL (c).

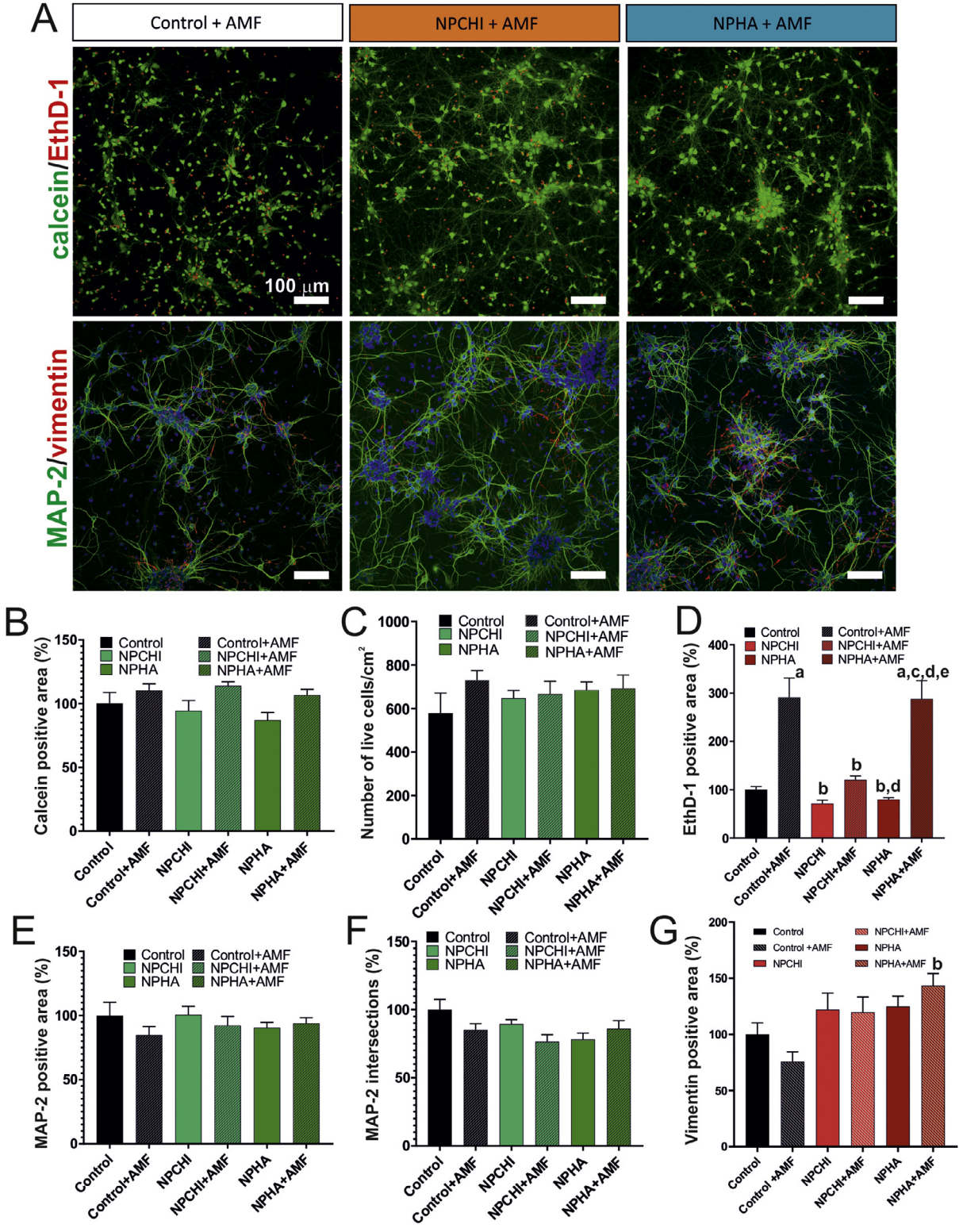

Fig. 4. Biological impact of magnetic stimulation in combination with the exposure to polymer-coated IONPs. Representative CLSM images of cell cultures exposed to an AMF (21 mT, 281kHz, 1 h) in the presence of IONPs (0.1 mg Fe/mL) for cell viability (A, top) and neural differentiation (A, bottom). Cell nuclei appear in blue in all images (Hoechst). Scale bars: 100 μm. Respective quantitative data for the positive area (B) and number (C) of live cells and the positive area of dead cells (D) and MAP-2 (E), the number of positive MAP-2^{+} intersections (F) and the positive area of vimentin (G). Statistics: one-way ANOVA followed by Games-Howell *post hoc* test (as dictated by Levene's test); N ≥ 3 experiments with duplicates per condition, n = 10 images per replicate. Significance: $p < 0.05$, comparisons with respect to control (a), control+AMF (b), NPCHI (c), NPCHI+AMF (d), and NPHA (e).

viable and highly interconnected neural networks over standard glass substrates. The slightly less favourable findings obtained at the highest concentration of NPHA could be related to some polymer excess in the culture, as supported by the larger hydrodynamic sizes found for NPHA but not for NPCHI. It has been shown that HA of high M_w, or even fragments of HA, can influence neural development by emitting quiescent signals in neurons and glial cells [70]. Moreover, Wilson *et al.* have demonstrated that the excess of HA in the neural environment can restrict excitatory synapse formation [71].

Encouraged by these positive findings from most of the conditions tested, we then analysed the impact of the exposure to an AMF (281 kHz, 21 mT, 1 h) in ENPC cultures incubated with the highest concentration of IONPs (0.1 mg Fe/mL) to maximize any eventual effect. The magnetic field selected in this work (16.8 kA/m, 281 kHz, being H x f = 4.7×10^9 A m^{-1} s^{-1}) is below the limit approved for localized magnetic hyperthermia therapies, using moderate field amplitude and frequency [23]. The former limit was established for the maximum field-frequency product as H × f = 4.85 × 10^8 A m^{-1} s^{-1}, called Atkinson–Brezovich limit, based on the feeling of discomfort in an irradiated patient, increased later on up to more than ten times for local treatments. Favourably, AMF application did not negatively impact either the area (one-way ANOVA, p = 0.212) or the number of live cells (one-way ANOVA, p = 0.556), which were maintained through all the conditions (Fig. 4A, top, and 4B,C). However, it significantly increased the quantity of dead cells in control and NPHA-exposed cells (one-way ANOVA followed by Games-Howell *post hoc* test, p ≤ 0.001***) (Fig. 4D). In this case, NPCHI seemed to display a clear and statistically significant protective effect against cell death after magnetic stimulation (one-way ANOVA followed by Games-Howell *post hoc* test, p = 0.005*** *vs* control+AMF and p = 0.002*** *vs* NPHA+AMF), in spite of its larger cell uptake. This finding is not surprising as CHI has been described as neuroprotective in neurons, especially against oxidative stress [37,72,73].

The biological effects of magnetic fields have not been unambiguously resolved yet. It is clear that cell responses depend on the field frequency and amplitude, as well as the presence or not of magnetic particles. Thus, while static or low frequency (in the Hz range) magnetic fields induced stimulation with no cytotoxic effects and enabled the development of neural networks [74], high frequency magnetic fields (in the kHz range) as those used in this work, may induce eddy currents, thermal heating or cell membrane deformation, even in absence of magnetic nanoparticles [75], and be responsible for the results presented here.

The impact of AMF stimulation on neural differentiation was also investigated. As previously found without magnetic stimulation, neuronal differentiation (MAP-2 labelling, one-way ANOVA, p = 0.662) and architectural connectivity (intersections of MAP-2-labelled neurites, one-way ANOVA, p > 0.061 in all cases) were maintained in all conditions, avoiding interferences with other features of neuronal maturation when applying the magnetic field in comparison to control samples (Fig. 4A, bottom, and 4E-F). Indeed, Rotherham *et al.* have already confirmed that neuronal differentiation in SH-SY5Y cells can be mechano-stimulated by the application of low frequency magnetic fields (≥ 25 mT, 1 Hz, 1–3 h), involving the activation of the *Wnt* signalling pathway [76]. Regarding vimentin$^+$ cells (Fig. 4A, bottom, and 4G), magnetic stimulation showed again a negligible impact on the area covered by non-neuronal cells except for a slight increase in the case of

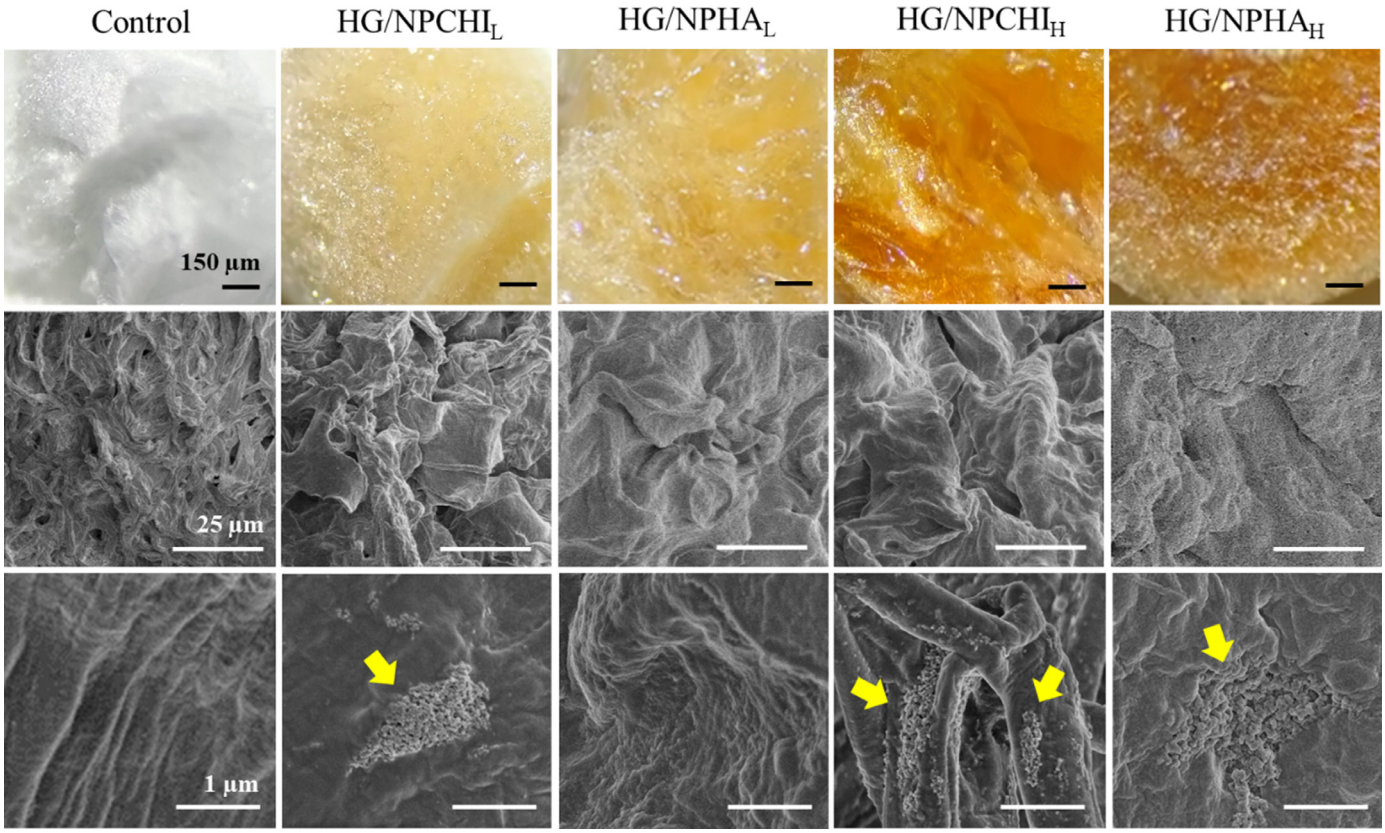

Fig. 5. Morphological characterization of collagen magnetic hydrogels doped with polymer-coated IONPs (NPCHI and NPHA). IONP doses were 0.04 and 0.5 mg Fe/mg polymer for collagen hydrogels loaded with NPCHI (HG/NPCHI$_L$ and HG/NPCHI$_H$, respectively) and 0.02 and 0.25 mg Fe/mg polymer for collagen hydrogels loaded with NPHA (HG/NPHA$_L$ and HG/NPHA$_H$, respectively). Macroscopic photographs were taken with a magnifying glass (top) and microscopic images were acquired by SEM at different magnifications (bottom). Location of IONPs observable on top and inside of collagen fibers are indicated with yellow arrows.

cells exposed to NPHA, which was only statistically significant in comparison to the insignificantly decreased control samples exposed to AMF (one-way ANOVA followed by Scheffé *post hoc* test, $p = 0.006^{**}$). Again, due to the noticeable variation in glial content obtained among cultures, this finding must be taken with care and be further investigated.

3.3. Characterization of magnetic hydrogels

Magnetic hydrogels were then fabricated by dispersing the polymer-coated IONPs developed within a collagen matrix (HG/NPX, being X either CHI or HA). The concentration range for each type of hydrogel was adjusted based on findings reported above for polymer-coated IONPs (0.04 and 0.5 mg Fe/mg polymer for HG/NPCHI$_L$ and HG/NPCHI$_H$, respectively; and 0.02 and 0.25 mg Fe/mg polymer for HG/NPHA$_L$ and HG/NPHA$_H$, respectively), with a lower range for NPHA due to the slight but noticeable decrease in cell viability and connectivity observed at higher doses. The selected IONP loading was sufficient to impact matrix density as, at a gross inspection, more compact hydrogels were obtained at higher doses of IONPs, regardless of the type (Fig. 5, top). As characterized by SEM, the resulting hybrid hydrogels showed a soft appearance and were constituted by a randomly porous and fibrous interconnected architecture (Fig. 5, middle and bottom), a consequence of the freeze-casting methodology used for their fabrication. Interestingly, pore size and fiber diameter were very alike among hydrogels with different IONP coating and concentration (Table 2 and Fig. S7), without statistically significant differences. By using TEM, we confirmed that both types of polymer-coated IONPs were found homogenously distributed throughout the totality of the hydrogel structure, becoming more abundant as IONP concentration increased (Figs. 6 and S8). This result confirms their complete colloidal stability in the collagen polymeric solution prior to freeze-casting for hydrogel formation, preliminary questioned by the slight evidences of IONP aggregation found under certain conditions (*e.g.,* a limited fraction of NPHA revealing much higher hydrodynamic sizes, certain IONP aggregates at the hydrogel surface visualized by SEM).

Table 2
Average fiber diameter and pore size of the different magnetic hydrogels fabricated. Quantitative values expressed as the mean ± SEM obtained from SEM micrographs. Not statistically significant differences were found among conditions.

Hydrogel type	Average fiber diameter (μm)	Average pore size (μm)
Control	1.96 ± 1.23	3.26 ± 7.19
HG/NPCHI$_L$	2.58 ± 1.40	6.41 ± 4.41
HG/NPCHI$_H$	2.27 ± 2.30	7.77 ± 5.96
HG/NPHA$_L$	2.18 ± 1.58	5.96 ± 4.29
HG/NPHA$_H$	1.45 ± 2.16	3.99 ± 5.59

Chemical characterization by FTIR analysis revealed the characteristic bands of collagen at 1660, 1079 and 1035 cm^{-1} in all hydrogels, corresponding to amides I, C-O and C-O-C groups, respectively (Fig. 7A) [77]. The other observed bands were assigned to the vibrations of functional groups of the polymers decorating the IONPs (CHI and HA), as previously indicated for those bands around 1150 - 1070 cm^{-1} (Fig. 1C). As expected, hydrogels prepared with a higher concentration of IONPs showed a higher intensity of the band near 560 cm^{-1}, which is related to the vibration of the Fe-O bond. As mentioned before, the band close to 1385 cm^{-1} corresponds to the presence of nitrate groups, only visible in those hydrogels with higher IONP concentration regardless of the polymer coating.

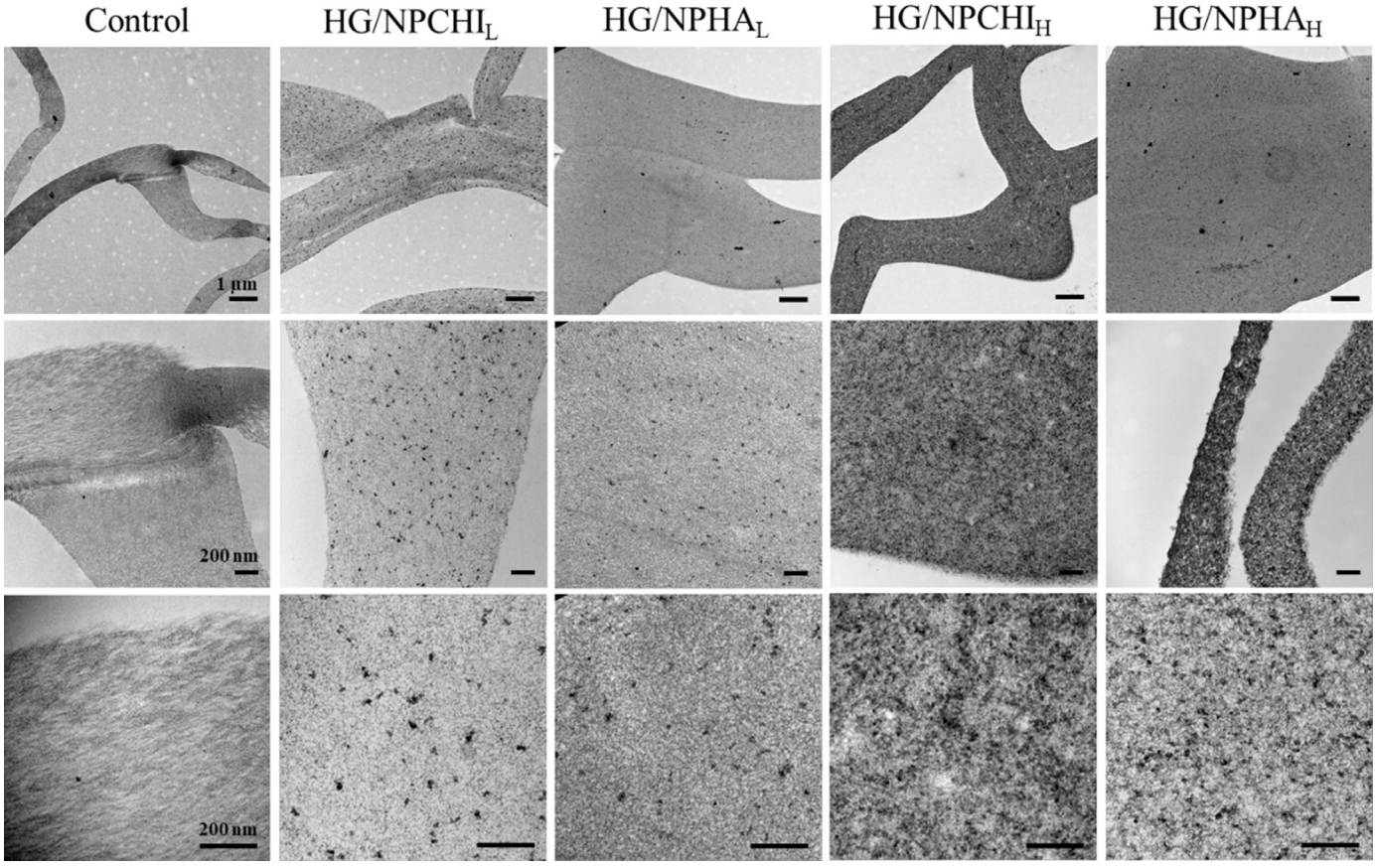

Fig. 6. Morphological characterization of hybrid magnetic hydrogels doped with polymer-coated IONPs (NPCHI and NPHA) by TEM. Black dots in the images are IONPs.

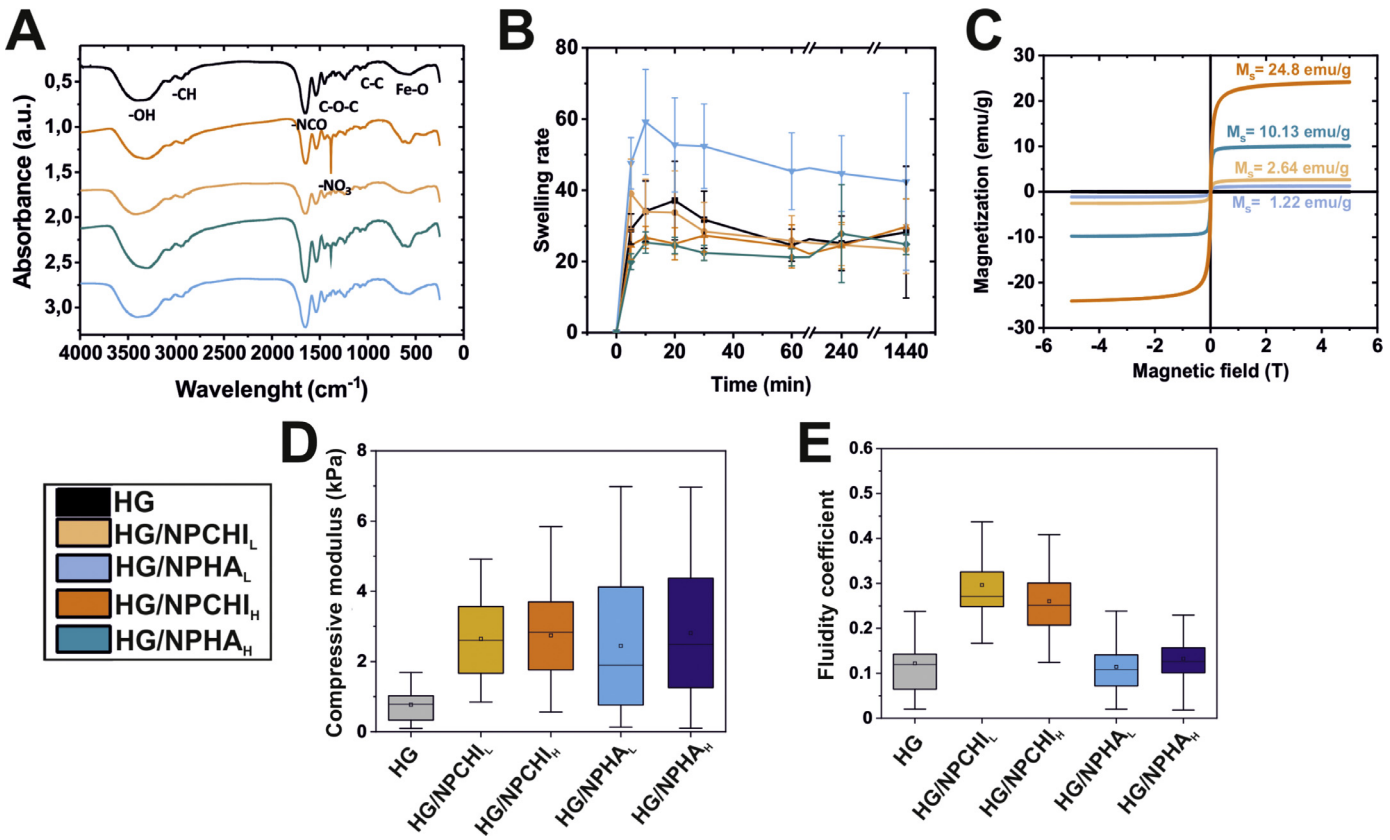

Fig. 7. Physicochemical characterization of magnetic hydrogels loaded with polymer-coated IONPs. FTIR spectra (A), swelling rate at different time points in distilled water at room temperature (B), magnetization curves at room temperature by VSM (C), compressive modulus (E_0, D), and fluidity coefficient (γ, E) obtained by AFM nanoindentation. Samples included: control collagen hydrogels (black), collagen hydrogels loaded with NPCHI at low (light orange) and high (dark orange) concentrations, and collagen hydrogels loaded with NPHA at low (light blue) and high (dark blue) concentrations.

The swelling capacity of the different magnetic hydrogels was then investigated (Fig. 7B). All hydrogels rapidly increased their volume and mass when submerged in distilled water until a plateau was rapidly reached after 10 min. Interestingly, low doses of IONPs, regardless of their polymer coating, augmented the hydrogel hydration degree. Contrarily, higher doses of IONPs reduced the swelling ratio of the hydrogels in comparison to control gels, as expected from the more compact structure found in the former ones. This is consistent with previous work in which higher concentrations of silica nanoparticles led to more rigid collagen/CHI/HA hydrogels [78–80]. Highly dependent on swelling, all magnetic hydrogels experienced a rapid degradation starting as early as 1-2 days in distilled water, demonstrating a clear impact of IONP loading in collagen hydrogel degradation. Specifically, hydrogel degradation proved to be dependent on IONP concentration, being those magnetic hydrogels with the lowest IONP dose the ones with smaller remaining weights after 30 days (Fig. S9). This result is in consonance with the swelling trend described above. Furthermore, hydrogels loaded with HA-coated IONPs were more rapidly degraded, in agreement with the superior capability of HA molecules to be hydrated. At 3 months, degradation features were clearly observable in all hydrogels, such as a higher porosity and abundant thin collagen fibers being torn from the remaining matrix, if any (Fig. S10). Focusing on the magnetic behavior of the hybrid hydrogels developed (Fig. 7C), we observed that the higher the IONPs concentration, the higher the magnetic signal found in the resulting hydrogel. Magnetization values as high as 24 emu/gFe were obtained for those hydrogels with the highest IONPs concentration (HG/NPCHI$_H$). Importantly, this magnetic response was found proportional to the IONP loading concentration (*i.e.,* a double concentration of IONPs duplicated the magnetic response, both for HG/NPCHI$_H$ and HG/NPHA$_H$). The magnetic response of the hydrogels was in all cases sufficient to ensure controlled movement of the gel through magnetic manipulation ($>$ 1 emu/gFe). Thus, by applying a moderate external magnetic field, the hydrogel could be directed, deformed or repositioned as desired.

In line with gross inspection and degradation findings, AFM nanoindentation measurements demonstrated that all hydrogels were very soft matrices. The addition of IONPs caused a threefold increase of the compressive modulus of the original collagen hydrogels (Fig. 7D), which ranged from 0.8 kPa to about 2.6 kPa, regardless of either the polymer coating or the dose of the IONPs. This result agreed with the initial gross appreciation of a clear stiffening of the collagen hydrogels when loaded with IONPs. Unexpectedly, we noted that the modulus hardly changed in the concentration range explored, so the stiffening associated with the addition of IONPs should be taking place at lower concentrations than those herein tested ($<$ 0.02 mgFe/mg polymer). Additionally, the fluidity coefficient (γ) measured the fluid character of the gel (Fig. 7E), ranging from 0 for an elastic solid to 1 for a perfect liquid [61]. The incorporation of NPCHI, loaded in the matrix at a higher concentration than NPHA, was found to markedly fluidize the collagen hydrogel (γ = 0.12 in control collagen hydrogels and γ = 0.27-0.29 in HG/NPCHI). However, this fluidization effect was not observed in any of the HG/NPHA hydrogels tested. As HA has a superior water adsorption capacity than CHI (anticipated to eventually assisting a more fluidic nature of the resulting hybrid hydrogels), we hypothesize this effect to be driven by weaker chemical interactions of NPCHI than NPHA with collagen molecules in the matrix.

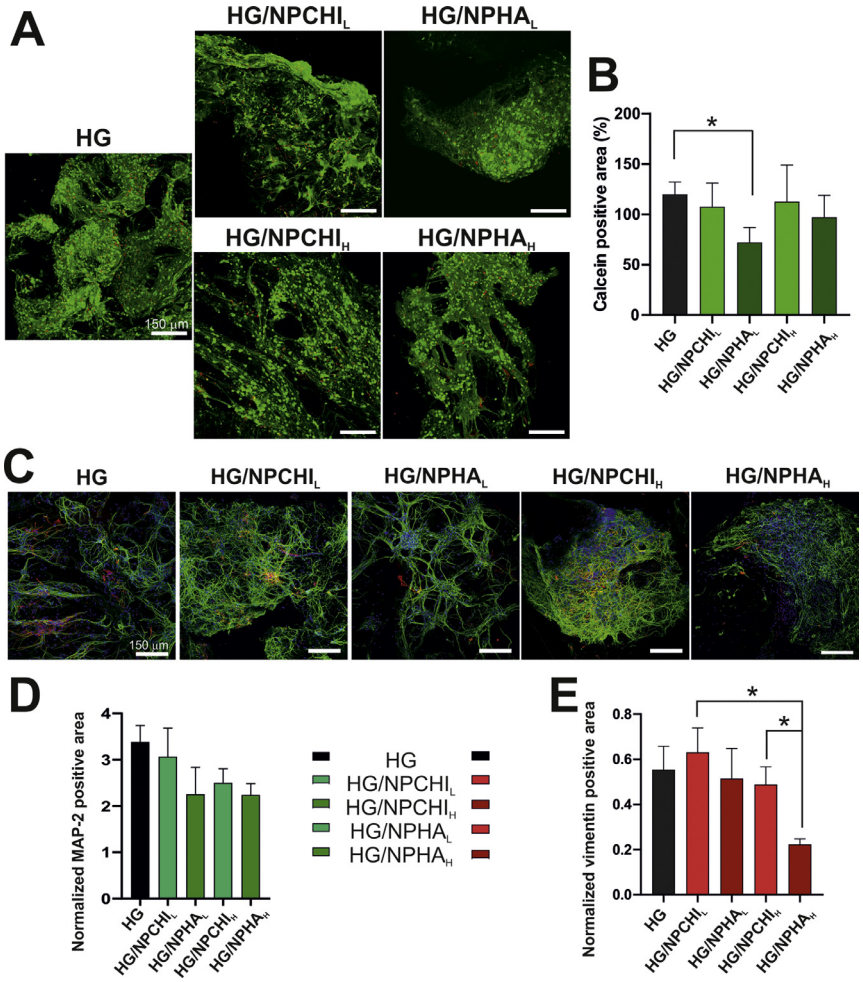

Fig. 8. Biological responses of ENPCs to magnetic collagen hydrogels loaded with polymer-coated IONPs (HG/NPCHI and HG/NPHA). Viability studies: Representative CLSM images (A) and corresponding quantification (B-C). Alive cells appear in green (calcein labelling) and dead cells in red (EthD-1 labelling). Reflection mode images are included for proper visualization of the respective hydrogel surface. Neural differentiation studies: Representative CLSM images (D) and corresponding quantification for MAP-2 (E; neuronal cells, green) and vimentin (F; non-neuronal cells including glial cells, red). In all images, cell nuclei appeared in blue (Hoechst). Statistics: one-way ANOVA followed by Games-Howell *post hoc* test (as dictated by Levene's test); N ≥ 3 experiments with duplicates per condition, n ≥ 3 images per replicate. Significance: $p < 0.05^*$ between groups connected by lines.

3.4. Biological responses of primary neural cells to magnetic hydrogels

The response of ENPCs to the magnetic hydrogels fabricated was then investigated. Morphological studies by SEM first revealed that these primary neural cells fully colonized and distributed homogeneously both on the surface and inside the pores of the hydrogels, with tight cell-cell and cell-collagen interactions (Fig. S11). The porous fibrillary structure of these scaffolds acted as the natural extracellular matrix supporting cell adhesion and growth. In the context of neural regeneration, this feature could be highly interesting for implantation, as cells from neighboring neural tissues could attach, grow and expand through the hydrogel to facilitate bridging.

Viability studies were then performed (Fig. 8A, B). No significant differences were found for calcein staining among hydrogels, regardless IONPs type or dose, except for HG/NPHA$_L$ hydrogels, which caused a significant decrease in the area of live cells just with respect to control ones (one-way ANOVA followed by Games-Howell *post hoc* test, $p = 0.037^*$). As the aspect of the colonized cells was found very alike among hydrogels, this decrease might be evidencing some other factors contributing to an overall poorer cell colonization of HG/NPHA$_L$ such as the faster degradation identified (Fig. 7D). The high bio-tolerance of these hybrid systems with primary neural cells was further corroborated when collagen hydrogels were doped with 8-fold higher doses of these IONPs than those described above. Specifically, ENPC viability was still preserved (Fig. S12A–C). Based on these findings, higher doses of IONPs could be loaded into these hydrogels if therapeutically needed without anticipating major toxicity issues. As for IONPs alone, neural differentiation of ENPCs was also evaluated in these magnetic hydrogels (Fig. 8C–E). First, the area covered by MAP-2$^+$ processes (mature neurons) was found similar among hydrogels, independently of IONP type and dose and in agreement with the results obtained with polymer-coated IONPs in suspension. In the case of non-neuronal cells, the area occupied by vimentin$^+$ processes was found again similar among conditions, except for HG/NPHA$_H$, in which neural cells decreased their differentiation to non-neuronal cells (*e.g.,* glial cells) with respect to both types of collagen hydrogels containing NPCHI (one-way ANOVA followed by Scheffé *post hoc* test, $p = 0.037^*$ *vs* HG/NPCHI$_L$ and $p = 0.042^*$ *vs* HG/NPCHI$_H$). This decrease was not correlated with results obtained with IONPs in suspension, in which no statistically significant differences were found among conditions, just a trend of decrease for NPCHI at the highest concentrations tested (Fig. 3). Therefore, the impact of this hybrid system on non-neuronal differentiation must be related to a synergistic effect of HA with col-

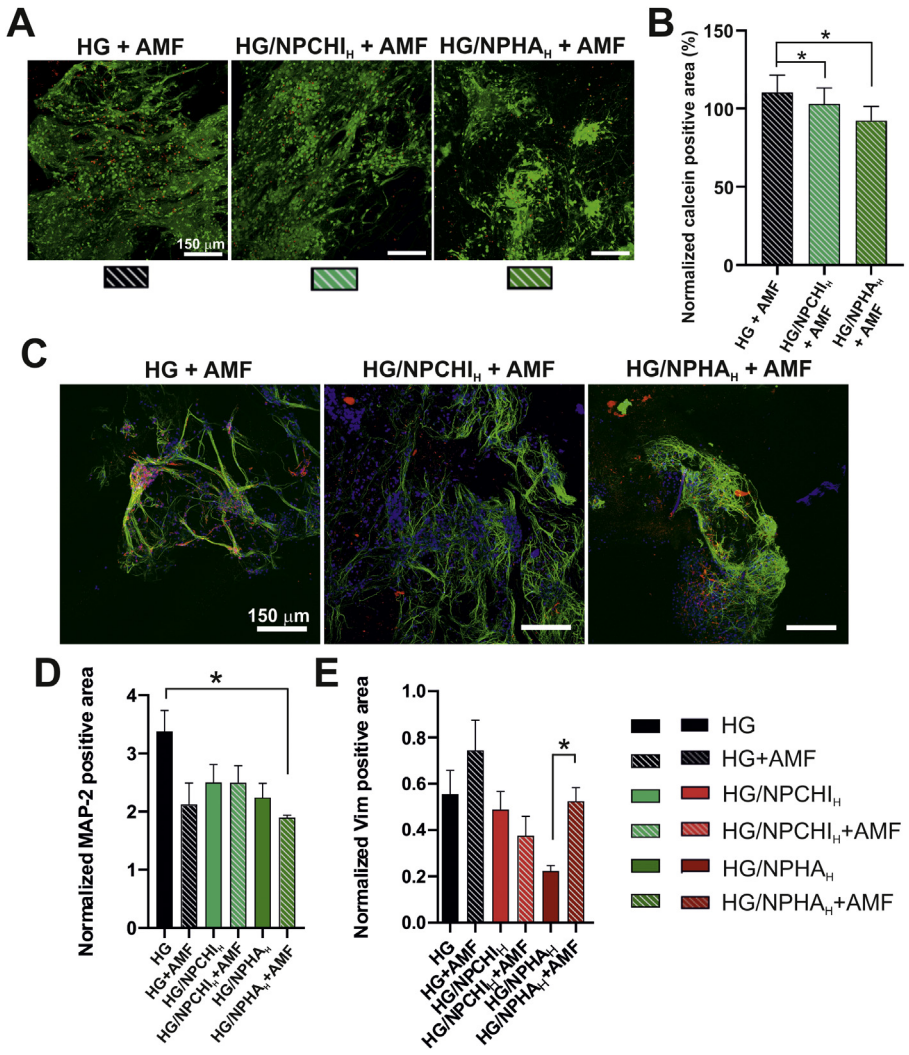

Fig. 9. Biological impact of magnetic stimulation on ENPCs cultured on magnetic hydrogels loaded with polymer-coated IONPs under AMF stimulation (21 mT, 281 kHz, 1 h). Viability studies: Representative CLSM images (A) and corresponding quantification (B). Alive cells appear in green (calcein labelling) and dead cells in red (EthD-1 labelling). Reflection mode images are also included for proper visualization of the respective hydrogel surface. Neural differentiation studies: Representative CLSM images (C) and corresponding quantification for MAP-2 (D; neuronal cells, green) and vimentin (E; non-neuronal cells including glial cells, red). In all images, cell nuclei appeared in blue (Hoechst). Statistics: one-way ANOVA followed by Games-Howell test (as dictated by Levene's test); N ≥ 3 experiments with duplicates per condition, n ≥ 3 images per replicate. Significance: $p < 0.05^*$ between groups connected by lines.

lagen, not induced by any of the components alone. Further studies are necessary to deepen on the impact of these IONPs when embedded in collagen hydrogels on neural phenotype maturation. Interestingly, it has been shown that modulating HA concentration can influence the elasticity of the developed hydrogels, thus impacting the development of the resulting neural networks [70]. Concretely, higher concentrations of HA lead to more elastic hydrogels that resulted in less migration, differentiation and branching of neural cells. In our case, the highest concentration of NPHA used to load the hydrogel (0.25 mg Fe/mg polymer) seemed sufficient to impact neural culture development regarding non-neuronal phenotypes.

Finally, we explored the impact that the application of an AMF could have on ENPCs cultured on magnetic hydrogels to approach their future use in magnetically triggered drug delivery strategies. Those hydrogels with the higher IONP concentration were selected to maximize responses. Regarding viability (Fig. 9A, B), the area positively labelled for live cells (calcein$^+$) significantly decreased in IONP-loaded hydrogels after AMF application, regardless of the IONP type, with respect to control hydrogels exposed to the same magnetic stimulation (one-way ANOVA followed by Games-Howell *post hoc* test, $p = 0.015^*$ for HG/NPCHI$_H$+AMF and $p = 0.035^*$ for HG/NPHA$_H$+AMF *vs* HG+AMF). However, values did not significantly differ from respective hydrogels without AMF, thus revealing a certain effect on the viability of these neural cells driven by the synergistic action of the IONPs and their actuation under an AMF. In the case of hydrogels doped with 8-fold higher doses of IONPs, viability was still preserved with respect to control behavior except for alive cells in HG/NPHA with and without magnetic stimulation (one-way ANOVA followed by Games-Howell *post hoc* test, $p = 0.008^{**}$) (Fig. S12D, E). In respect to neural differentiation (Fig. 9C–E), the area covered by neuronal cells was found again similar among hydrogels except for the amount of MAP-2$^+$ processes on HG/NPHA$_H$ under AMF, which were significantly reduced with respect to control hydrogels (one-way ANOVA followed by Scheffé *post hoc* test, $p = 0.023^*$). This slight decrease in MAP-2 was accompanied by a recovery of non-neuronal cells in these hydrogels (vimentin$^+$; one-way ANOVA followed by Games-Howell *post hoc* test, $p = 0.013^*$), being similar to control hydrogels for all the rest of conditions. Interestingly, this significant increase in vimentin$^+$ cells in HG/NPHA$_H$ under AMF agrees with results obtained with NPHA alone under AMF described above (Fig. 4), thus

pointing out a specific effect driven by magnetically actuated HA-coated IONPs on non-neuronal differentiation that requires further exploration in the future.

Taken together, hydrogels loaded with NPCHI seemed to provide a superior and more consistent response than those loaded with NPHA. Specifically, neural cell viability and neural differentiation (*i.e.,* MAP-2 and vimentin) showed higher values in HG/NPCHI for both low and high IONP doses in the absence of magnetic stimulation, reaching statistical significance with respect to HG/NPHA in several conditions such as viability for the low IONP concentration used and vimentin area. Under magnetic stimulation, the same trend was found, with the exception of vimentin area at the high IONP dose in HG/NPHA, similar to values obtained for HG/NPCHI. Moreover, certain degree of architectural instability and faster degradability of HG/NPHA at low IONP dose made them less favorable to work with. From a chemical point of view, the deacetylation degree of the CHI molecules used could be facilitating the interaction with neural cells, as previously described for Schwann cells [37,81]. In addition, its free protonated amino groups endow CHI the ability to bind to a wide range of natural and synthetic materials for functionalization and coating, likely benefiting cell adhesion and conferring a growth factors storage functionality. Regarding HA, it is known as a modulator of water-binding, ionic exchange, molecule size-dependent diffusion, and permeability of large molecules and cells [45–47]. However, its larger water uptake capabilities and lower availability of chemical groups might be responsible for this slightly inferior performance. These advantageous outcomes for HG/NPCHI over HG/NPHA can be also partially related to the higher fluidity of these hydrogels, as proved by the diffusion coefficient (γ), which can drive to a superior mechanical compliance with soft neural cells and tissues. Also, AMF application seemed to have a more noticeable impact on ENPC viability and differentiation when IONPs were loaded into the collagen matrices instead of in suspension. These findings might be indicating a facilitator role played by collagen on the mediation of biological interactions of polymer-coated IONPs with cell membrane receptors and molecules. Indeed, the confinement effect provided by the hydrogel could be exerting a role by propagating the impact of AMF application into a 3D environment. To this regard, it is important to investigate the kind of interactions that could be taking place inside the hydrogels when exposed to magnetic fields, both in the presence and absence of IONPs. For instance, IONPs could be aggregating [81], thus resulting in a less biocompatible environment for the establishment of well-formed neural networks. Importantly, this methodology was proved to be useful for the fabrication of other types of magnetic hydrogels, as those prepared by embedding NPCHI on CHI matrices (Fig. S13), which equally proved to acquire magnetic properties and sustain viable ENPC cultures. It is worth to mention that magneto-thermal stimulation can be used to control stem cell fate and to activate neuronal functions [82], typically occurring through the activation of temperature-sensitive transmembrane proteins [83,84]. However, magnetic nanoparticles under magnetic fields might also stimulate apoptotic pathways, which are not desired for tissue regeneration. Future work in our laboratory will intend to contribute to the elucidation of the impact of static and alternating magnetic stimulation on neural cells and tissues.

4. Conclusions

The natural polymers used to coat IONPs improved the response of primary neural cells by modulating the physico-chemical properties of the nanoparticles, for example, augmenting their hydrodynamic size and negative surface charge and tuning their magnetic responses depending on their respective hydration capacity. Those coated with chitosan (NPCHI) provided a superior neural cell response than those with hyaluronic acid (NPHA), including larger IONP uptake and a wider concentration-ranged viability and neural differentiation. Furthermore, the application of an AMF did not seem to impact negatively ENPC growth and development in the presence of IONPs in suspension, making these polymer-coated IONPs potentially useful nanocarriers. Additionally, they were proved to be homogenously distributed in collagen hydrogels, tuning their physico-chemical properties through the variation of IONP dose, such as compactness, degradation rate, responsiveness to magnetic stimuli, and nanomechanical properties. By incorporating these polymer-coated IONPs, we have fabricated magnetic hydrogels which can be controlled by using an AMF. These hydrogels were fully colonized by primary neural cells and proved to be biocompatible. Also, slight but significant differences in neural cell responses suggested a differential impact of the polymer coating of IONPs on the interactions with the collagen matrix, thus providing a wider set of controllable parameters to reach desire outcomes. As for IOPNs alone, NPCHI-loaded hydrogels demonstrated a superior cell response for which their higher fluidity might be contributing. This methodology was further proved successful for the fabrication of alternative magnetic hydrogels composed of NPCHI embedded into a chitosan matrix. Overall, the positive findings presented herein encourage the optimization of these hybrid materials as potent carrier platforms for neural repair. The incorporation of therapeutic agents into these soft and highly biocompatible magnetic hydrogels could enable the spatial and temporal control of the release of drugs by the application of an external magnetic field, being magnetic stimulation itself already incorporated in the clinical practice for therapeutic purposes. These systems could open a new avenue for the development of personalized therapies in patients with the need of neural repair such as those affected by spinal cord injury, traumatic brain injury and tumors to be resected at the central nervous tissue, among others. The promising but still early stage of this research encourages further investigation to bring these useful nanotechnology-based tools closer to their clinical application.

Data availability

All data are available in the main text or the supplementary material. Additional raw and processed data required to reproduce these findings will be available to download from DIGITAL.CSIC upon acceptance and may also be requested from the authors.

Funding sources

This work has received funding from the European Union's Horizon Europe research and Innovation Programme under grant agreement No. 101098597. It has been also supported by grant PID2020-113480RB-I00 funded by MCIN/AEI/10.13039/501100011033/.

Declaration of competing interest

The authors declare that they have no known competing financial interests or personal relationships that could have appeared to influence the work reported in this paper.

The authors declare the following financial interests/personal relationships which may be considered as potential competing interests:

Maria Concepcion Serrano reports financial support was provided by European Union Horizon Europe research and Innovation Programme. Maria Concepcion Serrano reports financial support was provided by Agencia Estatal de Investigacion MCIN of Spain.

Acknowledgements

The Advanced Light Microscopy Service at the *Centro Nacional de Biotecnología* (CNB–CSIC) is acknowledged for assistance with confocal microscopy studies, the Electron Microscopy Service at the *Centro de Biología Molecular Severo Ochoa* (CBMSO, CSIC-UAM) for TEM studies, the Scanning Electron Microscopy Service at the *Instituto de Micro y Nanotecnología* (IMN-CSIC) for FESEM, and technical personnel at the *Instituto de Ciencia de Materiales de Madrid* (ICMM-CSIC) for ICP-OES, FTIR and XRD analyses. Authors are also thankful to the *Servicio Interdepartamental de Investigación* at the *Universidad Autónoma de Madrid* for assistance with SEM studies. The MiNa Laboratory at IMN-CSIC acknowledges its funding from CM (project S2018/NMT-4291 TEC2SPACE), MINECO (project CSIC13-4E-1794) and EU (FEDER, FSE). Authors are grateful to Inmaculada Aranaz from the *Universidad Complutense de Madrid* for assistance with chitosan characterization studies. EB acknowledges *Ministerio de Ciencia e Innovación* of Spain for an FPI fellowship associated to grant PID2020-113480RB-I00. MTT acknowledges *Comunidad de Madrid* for a contract from the *Programa Investigo* and NVG and JMR acknowledge *CSIC* for a JAE-Intro ICU and a JAE-Intro ICU Nanomed CSIC Hub fellowships, respectively.

Supplementary materials

Supplementary material associated with this article can be found, in the online version, at doi:10.1016/j.actbio.2024.01.030.

References

[1] M. Gomez-Florit, A. Pardo, R.M.A. Domingues, A.L. Graça, P.S. Babo, R.L. Reis, M.E. Gomes, Natural-based hydrogels for tissue engineering applications, Molecules. 25 (2020) 5858, doi:10.3390/molecules25245858.
[2] A. Pardo, M. Gómez-Florit, S. Barbosa, P. Taboada, R.M.A. Domingues, M.E. Gomes, Magnetic nanocomposite hydrogels for tissue engineering: design concepts and remote actuation strategies to control cell fate, ACS Nano 15 (2021) 175–209, doi:10.1021/acsnano.0c08253.
[3] R. Kumar, K.R. Aadil, S. Ranjan, V.B. Kumar, Advances in nanotechnology and nanomaterials-based strategies for neural tissue engineering, J. Drug Deliv. Sci. Technol. 57 (2020) 101617, doi:10.1016/J.JDDST.2020.101617.
[4] P. Kesharwani, A. Bisht, A. Alexander, V. Dave, S. Sharma, Biomedical applications of hydrogels in drug delivery system: an update, J. Drug Deliv. Sci. Technol. 66 (2021) 102914, doi:10.1016/J.JDDST.2021.102914.
[5] Y. Sun, D. Nan, H. Jin, X. Qu, Recent advances of injectable hydrogels for drug delivery and tissue engineering applications, Polym. Test. 81 (2020) 106283, doi:10.1016/J.POLYMERTESTING.2019.106283.
[6] S. Grijalvo, R. Eritja, D. Díaz, On the race for more stretchable and tough hydrogels, Gels 5 (2019) 24, doi:10.3390/gels5020024.
[7] M.M. El Sayed, Production of polymer hydrogel composites and their applications, J. Polym. Environ. 31 (2023) 2855–2879 https://link.springer.com/article/10.1007/s10924-023-02796-z.
[8] H. Gregory, J.B. Phillips, Materials for peripheral nerve repair constructs: natural proteins or synthetic polymers? Neurochem. Int. 143 (2021) 104953, doi:10.1016/j.neuint.2020.104953.
[9] S. Naahidi, M. Jafari, M. Logan, Y. Wang, Y. Yuan, H. Bae, B. Dixon, P. Chen, Biocompatibility of hydrogel-based scaffolds for tissue engineering applications, Biotechnol. Adv. 35 (2017) 530–544, doi:10.1016/J.BIOTECHADV.2017.05.006.
[10] K. Elkhoury, M. Morsink, L. Sanchez-Gonzalez, C. Kahn, A. Tamayol, E. Arab-Tehrany, Biofabrication of natural hydrogels for cardiac, neural, and bone Tissue engineering Applications, Bioact. Mater. 6 (2021) 3904–3923, doi:10.1016/J.BIOACTMAT.2021.03.040.
[11] E. Barrett-Catton, M.L. Ross, P. Asuri, Multifunctional hydrogel nanocomposites for biomedical applications, Polymers 13 (2021) 856–870, doi:10.3390/POLYM13060856.
[12] W.H. Huang, S.L. Ding, X.Y. Zhao, K. Li, H.T. Guo, M.Z. Zhang, Q. Gu, Collagen for neural tissue engineering: materials, strategies, and challenges, Mater. Today Bio 20 (2023) 100639, doi:10.1016/j.mtbio.2023.100639.
[13] H. Samadian, H. Maleki, A. Fathollahi, M. Salehi, S. Gholizadeh, H. Derakhshankhah, Z. Allahyari, M. Jaymand, Naturally occurring biological macromolecules-based hydrogels: potential biomaterials for peripheral nerve regeneration, Int. J. Biol. Macromol. 154 (2020) 795–817, doi:10.1016/J.IJBIOMAC.2020.03.155.
[14] R. Parenteau-Bareil, R. Gauvin, F. Berthod, Collagen-based biomaterials for tissue engineering applications, Materials 3 (2010) 1863–1887, doi:10.3390/ma3031863.
[15] E. Guler, E. Beyzanur Polat, M. Emin Cam, Drug delivery systems for neural tissue engineering, in: Biomaterials for Neural Tissue Engineering, Woodhead Publishing Series in Biomaterials, 2023, pp. 221–268, doi:10.1016/B978-0-323-90554-1.00012-4.
[16] O. Turan, P. Bielecki, V. Perera, M. Lorkowski, G. Covarrubias, K. Tong, A. Yun, A. Rahmy, T. Ouyang, S. Raghunathan, R. Gopalakrishnan, M.A. Griswold, K.B. Ghaghada, P.M. Peiris, E. Karathanasis, Delivery of drugs into brain tumors using multicomponent silica nanoparticles, Nanoscale 11 (2019) 11910–11921, doi:10.1039/C9NR02876E.
[17] A. Mittal, I. Roy, S. Gandhi, Magnetic nanoparticles: an overview for biomedical applications, Magnetochemistry 8 (2022) 107, doi:10.3390/magnetochemistry8090107.
[18] W. Wu, Z. Wu, T. Yu, C. Jiang, W.S. Kim, Recent progress on magnetic iron oxide nanoparticles: synthesis, surface functional strategies and biomedical applications, Sci. Technol. Adv. Mater. 16 (2015) 023501, doi:10.1088/1468-6996/16/2/023501.
[19] A.H. Lu, E.L. Salabas, F. Schüth, Magnetic nanoparticles: synthesis, protection, functionalization, and application, Angew. Chem. Int. Ed. 46 (2007) 1222–1244, doi:10.1002/anie.200602866.
[20] J. Ovejero, E. Wang, S. Veintemillas-Verdaguer, M. Morales, A. Sorolla, Nanoparticles for neural applications„ in: E. López-Dolado, MC. Serrano (Eds.), Engineering Biomaterials for Neural Applications, Springer Nature, 2022, pp. 149–184, doi:10.1007/978-3-030-81400-7.
[21] O. Veiseh, J.W. Gunn, M. Zhang, Design and fabrication of magnetic nanoparticles for targeted drug delivery and imaging, Adv. Drug Deliv. Rev. 62 (2010) 284–304 https://www.sciencedirect.com/science/article/abs/pii/S0169409x09003408?via%3Dihub.
[22] S.M. Dadfar, K. Roemhild, N.I. Drude, S. von Stillfried, R. Knüchel, F. Kiessling, T. Lammers, Iron oxide nanoparticles: diagnostic, therapeutic and theranostic applications, Adv. Drug Deliv. Rev. 138 (2019) 302–325, doi:10.1016/j.addr.2019.01.005.
[23] D. Egea-Benavente, J.G. Ovejero, M.D.P. Morales, D.F. Barber, Understanding MNPs behaviour in response to AMF in biological milieus and the effects at the cellular level: implications for a rational design that drives magnetic hyperthermia therapy toward clinical implementation, Cancers 13 (2021) 4583, doi:10.3390/CANCERS13184583.
[24] N. Massironi, M. Colombo, C. Cosentino, L. Fiandra, M. Mauri, Y. Kayal, F. Testa, G. Torri, E. Urso, E. Vismara, I. Vlodavsky, Heparin–superparamagnetic iron oxide nanoparticles for theranostic applications, Molecules 27 (2022) 7116, doi:10.3390/molecules27207116.
[25] E.H. Fragal, V.H. Fragal, E.P. Silva, A.T. Paulino, E.C. da Silva Filho, M.R. Mauricio, R. Silva, A.F. Rubira, E.C. Muniz, Magnetic-responsive polysaccharide hydrogels as smart biomaterials: synthesis, properties, and biomedical applications, Carbohydr. Polym. 292 (2022) 119665, doi:10.1016/j.carbpol.2022.119665.
[26] Q. Shi, H. Liu, D. Tang, Y. Li, X. Li, F. Xu, Bioactuators based on stimulus-responsive hydrogels and their emerging biomedical applications, NPG Asia Mater. 11 (2019) 64, doi:10.1038/s41427-019-0165-3.
[27] H. Jafari, Z. Atlasi, G.R. Mahdavinia, S. Hadifar, M. Sabzi, Magnetic κ-carrageenan/chitosan/montmorillonite nanocomposite hydrogels with controlled sunitinib release, Mater. Sci. Eng. C 124 (2021) 112042, doi:10.1016/j.msec.2021.112042.
[28] S. Kondaveeti, A.T.S. Semeano, D.R. Cornejo, H. Ulrich, D.F.S. Petri, Magnetic hydrogels for levodopa release and cell stimulation triggered by external magnetic field, Colloids Surf. B Biointerfaces 167 (2018) 415–424, doi:10.1016/j.colsurfb.2018.04.040.
[29] C. Kim, H. Kim, H. Park, K.Y. Lee, Controlling the porous structure of alginate ferrogel for anticancer drug delivery under magnetic stimulation, Carbohydr. Polym. 223 (2019) 115045, doi:10.1016/j.carbpol.2019.115045.
[30] C.S. Lacko, I. Singh, M.A. Wall, Magnetic particle templating of hydrogels: engineering naturally derived hidrogel scaffolds with 3D aligned microarchitecture for nerve repair, J. Neural Eng. 17 (2020) 016057, doi:10.1088/1741-2552/ab4a22.
[31] M. Antman-Passig, O. Shefi, Remote magnetic orientation of 3D collagen hydrogels for directed neuronal regeneration, Nano Lett. 16 (2016) 2567–2573, doi:10.1021/acs.nanolett.6b00131.
[32] A. Omidinia-Anarkoli, S. Boesveld, U. Tuvshindorj, J.C. Rose, T. Haraszti, L. De Laporte, An injectable hybrid hydrogel with oriented short fibers induces unidirectional growth of functional nerve cells, Small 13 (2017) 101002, doi:10.1002/smll.201702207.
[33] C.Y. Yang, Z. Meng, K. Yang, External magnetic field non-invasively stimulates spinal cord regeneration in rat via a magnetic-responsive aligned fibrin hydrogel, Biofabrication 15 (2023) 1758–5090, doi:10.1088/1758-5090/acdbec.
[34] W.C. Huang, C.C. Lin, T.W. Chiu, S.Y. Chen, 3D gradient and linearly aligned magnetic microcapsules in nerve guidance conduits with remotely spatiotemporally controlled release to enhance peripheral nerve repair, ACS. Appl. Mater. Interfaces 14 (2022) 46188–46200, doi:10.1021/acsami.2c11362.
[35] W. Wei, L. Bo, G. Changyou, Modulating the differentiation of BMSCs by surface properties of biomaterials, Prog. Chem. 23 (2011) 2160–2168.
[36] S. Del Sol-Fernández, P. Martínez-Vicente, P. Gomollón-Zueco, C. Castro-Hinojosa, L. Gutiérrez, R.M. Fratila, M. Moros, Magnetogenetics: remote activation of cellular functions triggered by magnetic switches, Nanoscale 14 (2022) 2091–2118, doi:10.1039/D1NR06303K.
[37] B. Farhadihosseinabadi, A. Zarebkohan, M. Eftekhary, M. Heiat, M. Moosazadeh Moghaddam, M. Gholipourmalekabadi, Crosstalk between chitosan and cell signaling pathways, Cell. Mol. Life Sci. 76 (2019) 2697–2718, doi:10.1007/s00018-019-03107-3.
[38] D.D. Ojeda-Hernández, A.A. Canales-Aguirre, J. Matias-Guiu, U. Gomez-Pinedo, J.C. Mateos-Díaz, Potential of chitosan and its derivatives for biomedical appli-

cations in the central nervous system, Front. Bioeng. Biotechnol. 8 (2020) 389, doi:10.3389/fbioe.2020.00389.
[39] X. Xing, Y. Han, H. Cheng, Biomedical applications of chitosan/silk fibroin composites: a review, Int. J. Biol. Macromol. 240 (2023) 124407, doi:10.1016/j.ijbiomac.2023.124407.
[40] E.M.M. Ali, A.A. Elashkar, H.Y. El-Kassas, E.I. Salim, Methotrexate loaded on magnetite iron nanoparticles coated with chitosan: biosynthesis, characterization, and impact on human breast cancer MCF-7 cell line, Int. J. Biol. Macromol. 120 (2018) 1170–1180, doi:10.1016/J.IJBIOMAC.2018.08.118.
[41] S. Ayyanaar, C. Balachandran, R.C. Bhaskar, M.P. Kesavan, S. Aoki, R.P. Raja, J. Rajesh, T.J. Webster, G. Rajagopal, ROS-responsive chitosan coated magnetic iron oxide nanoparticles as potential vehicles for targeted drug delivery in cancer therapy, Int. J. Nanomed. 15 (2020) 3333–3346, doi:10.2147/IJN.S249240.
[42] H.S. Budi, S. Izadi, A. Timoshin, S.H. Asl, B. Beyzai, A. Ghaderpour, F. Alian, F.S. Eshaghi, S.M. Mousavi, B. Rafiee, A. Nikkhoo, A. Ahmadi, H. Hassannia, M. Ahmadi, M. Sojoodi, F. Jadidi-Niaragh, Blockade of HIF-1α and STAT3 by hyaluronate-conjugated TAT-chitosan-SPION nanoparticles loaded with siRNA molecules prevents tumor growth, Nanomedicine 34 (2021) 102373, doi:10.1016/J.NANO.2021.102373.
[43] L. Gholami, M. Tafaghodi, B. Abbasi, M. Daroudi, R.K. Oskuee, Preparation of superparamagnetic iron oxide/doxorubicin loaded chitosan nanoparticles as a promising glioblastoma theranostic tool, J. Cell. Physiol. 234 (2019) 1547–1559, doi:10.1002/JCP.27019.
[44] S.H. Bakhru, E. Altiok, C. Highley, D. Delubac, J. Suhan, T.K. Hitchens, C. Ho, S. Zappe, Enhanced cellular uptake and long-term retention of chitosan-modified iron-oxide nanoparticles for MRI-based cell tracking, Int. J. Nanomed. 7 (2012) 4613–4623, doi:10.2147/IJN.S28294.
[45] G. Abatangelo, V. Vindigni, G. Avruscio, L. Pandis, P. Brun, Hyaluronic acid: redefining its role, Cells 9 (2020) 1743, doi:10.3390/cells9071743.
[46] M.A. Selyanin, P.Y. Boykov, V.N. Khabarov, F. Polyak, Hyaluronic Acid, Wiley, 2015, doi:10.1002/9781118695920.
[47] A. Fallacara, E. Baldini, S. Manfredini, S. Vertuani, Hyaluronic acid in the third millennium, Polymers 10 (2018) 701, doi:10.3390/polym10070701.
[48] M. Soleymani, M. Velashjerdi, Z. Shaterabadi, A. Barati, One-pot preparation of hyaluronic acid-coated iron oxide nanoparticles for magnetic hyperthermia therapy and targeting CD44-overexpressing cancer cells, Carbohydr. Polym. 237 (2020) 116130, doi:10.1016/J.CARBPOL.2020.116130.
[49] M. Kamat, K. El-Boubbou, D.C. Zhu, T. Lansdell, X. Lu, W. Li, X. Huang, Hyaluronic acid immobilized magnetic nanoparticles for active targeting and imaging of macrophages, Bioconjug. Chem. 21 (2010) 2128–2135, doi:10.1021/bc100354m.
[50] E. Vismara, C. Bongio, A. Coletti, R. Edelman, A. Serafini, M. Mauri, R. Simonutti, S. Bertini, E. Urso, Y.G. Assaraf, Y.D. Livney, Albumin and hyaluronic acid-coated superparamagnetic iron oxide nanoparticles loaded with paclitaxel for biomedical applications, Molecules. 22 (2017) 1030, doi:10.3390/MOLECULES22071030.
[51] H. Unterweger, R. Tietze, C. Janko, J. Zaloga, S. Lyer, S. Dürr, N. Taccardi, O.M. Goudouri, A. Hoppe, D. Eberbeck, D.W. Schubert, A.R. Boccaccini, C. Alexiou, Development and characterization of magnetic iron oxide nanoparticles with a cisplatin-bearing polymer coating for targeted drug delivery, Int. J. Nanomed. 9 (2014) 3659–3676, doi:10.2147/IJN.S63433.
[52] L.R. Nih, S. Gojgini, S.T. Carmichael, T. Segura, Dual-function injectable angiogenic biomaterial for the repair of brain tissue following stroke, Nat. Mater. 17 (2018) 642–651, doi:10.1038/s41563-018-0083-8.
[53] D.J. Craik, P.M. Griffiths, B.L. Appl, E.E. Bibik, F. Efremov, I.S. Lavrov, R.M. Del Vecchio, J. Sefko, in: Physics, 39, Freeman, 1981, p. 279. vol., p..
[54] R. Costo, V. Bello, C. Robic, M. Port, J.F. Marco, M.P. Morales, S. Veintemillas-Verdaguer, Ultrasmall iron oxide nanoparticles for biomedical applications: improving the colloidal and magnetic properties, Langmuir 28 (2012) 178–185 https://pubs.acs.org/doi/10.1021/la203428z.
[55] M. Zahraei, M. Marciello, A. Lazaro-Carrillo, A. Villanueva, F. Herranz, M. Talelli, R. Costo, A. Monshi, D. Shahbazi-Gahrouei, M. Amirnasr, B. Behdadfar, M.P. Morales, Versatile theranostics agents designed by coating ferrite nanoparticles with biocompatible polymers, Nanotechnology 27 (2016) 255702, doi:10.1088/0957-4484/27/25/255702.
[56] R.A.A. Muzzarelli, R. Rocchetti, Determination of the degree of acetylation of chitosans by first derivative ultraviolet spectrophotometry, Carbohydr. Polym. 5 (1985) 461–472, doi:10.1016/0144-8617(85)90005-0.
[57] H.N. Koo, H.J. Jeong, S.H. Hong, J.H. Choi, N.H. An, H.M. Kim, High molecular weight water-soluble chitosan protects against apoptosis induced by serum starvation in human astrocytes, J. Nutr. Biochem. 13 (2002) 245–249 https://www.sciencedirect.com/science/article/abs/pii/S0955286301002182?via%3Dihub.
[58] Z. Cao, R.J. Gilbert, W. He, Simple agarose-chitosan gel composite system for enhanced neuronal growth in three dimensions, Biomacromolecules 10 (2009) 2954–2959, doi:10.1021/bm900670n.
[59] X. Wang, J. Miao, C. Yan, R. Ge, T. Liang, E. Liu, Q. Li, Chitosan attenuates dibutyltin-induced apoptosis in PC12 cells through inhibition of the mitochondria-dependent pathway, Carbohydr. Polym. 151 (2016) 996–1005, doi:10.1016/j.carbpol.2016.06.053.
[60] J.G. Ovejero, I. Armenia, D. Serantes, S. Veintemillas-Verdaguer, N. Zeballos, F. López-Gallego, C. Grüttner, J.M. de la Fuente, M.P. Morales, V. Grazu, Selective magnetic nanoheating: combining iron oxide nanoparticles for multi-hot-spot induction and sequential regulation, Nano Lett. 21 (2021) 7213–7220, doi:10.1021/acs.nanolett.1c02178.
[61] P.D. García, C.R. Guerrero, R. García, Nanorheology of living cells measured by AFM-based force–distance curves, Nanoscale 12 (2020) 9133–9143 https://pubs.rsc.org/en/content/articlelanding/2020/nr/c9nr10316c.
[62] M.C. Serrano, J. Patiño, C. García-Rama, M.L. Ferrer, J.L.G. Fierro, A. Tamayo, J.E. Collazos-Castro, F. del Monte, M.C. Gutiérrez, 3D free-standing porous scaffolds made of graphene oxide as substrates for neural cell growth, J. Mater. Chem. B 2 (2014) 5698, doi:10.1039/C4TB00652F.
[63] A. Domínguez-Bajo, J.M. Rosa, A. González-Mayorga, B.L. Rodilla, A. Arché-Núñez, E. Benayas, P. Ocón, L. Pérez, J. Camarero, R. Miranda, M.T. González, J. Aguilar, E. López-Dolado, M.C. Serrano, Nanostructured gold electrodes promote neural maturation and network connectivity, Biomaterials 279 (2021) 121186, doi:10.1016/j.biomaterials.2021.121186.
[64] M.F. Queiroz, K.R.T. Melo, D.A. Sabry, G.L. Sassaki, H.A.O. Rocha, Does the use of chitosan contribute to oxalate kidney stone formation? Mar. Drugs 13 (2015) 141–158, doi:10.3390/md13010141.
[65] W.F. Wolkers, A.E. Oliver, F. Tablin, J.H. Crowe, A Fourier-transform infrared spectroscopy study of sugar glasses, Carbohydr. Res. 339 (2004) 1077–1085, doi:10.1016/j.carres.2004.01.016.
[66] M.M. Yallapu, N. Chauhan, S.F. Othman, V. Khalilzad-Sharghi, M.C. Ebeling, S. Khan, M. Jaggi, S.C. Chauhan, Implications of protein corona on physico-chemical and biological properties of magnetic nanoparticles, Biomaterials 46 (2015) 1–12, doi:10.1016/j.biomaterials.2014.12.045.
[67] A. Rampino, M. Borgogna, P. Blasi, B. Bellich, A. Cesàro, Chitosan nanoparticles: preparation, size evolution and stability, Int. J. Pharm. 455 (2013) 219–228, doi:10.1016/j.ijpharm.2013.07.034.
[68] C. Varan, E. Bilensoy, Cationic PEGylated polycaprolactone nanoparticles carrying post-operation docetaxel for glioma treatment, Beilstein J. Nanotechnol. 8 (2017) 1446–1456, doi:10.3762/bjnano.8.144.
[69] E. Benayas, A. Espinosa, M.T. Portolés, V. Vila-Del Sol, M.P. Morales, M.C. Serrano, Cellular and molecular processes are differently influenced in primary neural cells by slight changes in the physicochemical properties of multicore magnetic nanoparticles, ACS Appl. Mater. Interfaces 15 (2023) 17726–17741, doi:10.1021/ACSAMI.3C02729/ASSET/IMAGES/LARGE/AM3C02729_0007.JPEG.
[70] S.K. Seidlits, Z.Z. Khaing, R.R. Petersen, J.D. Nickels, J.E. Vanscoy, J.B. Shear, C.E. Schmidt, The effects of hyaluronic acid hydrogels with tunable mechanical properties on neural progenitor cell differentiation, Biomaterials 31 (2010) 3930–3940, doi:10.1016/j.biomaterials.2010.01.125.
[71] E. Wilson, W. Knudson, K. Newell-Litwa, Hyaluronan regulates synapse formation and function in developing neural networks, Sci. Rep. 10 (2020) 16459, doi:10.1038/s41598-020-73177-y.
[72] B. Chen, J. Li, R.B. Borgens, Neuroprotection by chitosan nanoparticles in oxidative stress-mediated injury, BMC Res. Notes 11 (2018) 49, doi:10.1186/s13104-018-3162-7.
[73] N.L. Pop, A. Nan, A.E. Urda-Cimpean, A. Florea, V.A. Toma, R. Moldovan, N. Decea, D. Rodica Mitrea, R. Orasan, Chitosan functionalized magnetic nanoparticles to provide neural regeneration and recovery after experimental model induced peripheral nerve injury, Biomolecules. 11 (2021) 676, doi:10.3390/biom11050676.
[74] R. Plen, A. Smith, O. Blum, O. Aloni, U. Locker, Z. Shapira, S. Margel, O. Shefi, Bioengineering 3D neural networks using magnetic manipulations, Adv. Funct. Mater. 32 (2022) 2204925, doi:10.1002/adfm.202204925.
[75] V.N. Binhi, A.B. Rubin, Theoretical concepts in magnetobiology after 40 years of research, Cells 11 (2022) 274 https://www.mdpi.com/2073-4409/11/2/274.
[76] M. Rotherham, T. Nahar, T. Goodman, N. Telling, M. Gates, A. El Haj, Magnetic mechanoactivation of Wnt signaling augments dopaminergic differentiation of neuronal cells, Adv. Biosyst. 3 (2019) 1900091, doi:10.1002/adbi.201900091.
[77] K. Belbachir, R. Noreen, G. Gouspillou, C. Petibois, Collagen types analysis and differentiation by FTIR spectroscopy, Anal. Bioanal. Chem. 395 (2009) 829–837, doi:10.1007/s00216-009-3019-y.
[78] J. Lewandowska-Łańcucka, A. Gilarska, A. Buła, W. Horak, A. Łatkiewicz, M. Nowakowska, Genipin crosslinked bioactive collagen/chitosan/hyaluronic acid injectable hydrogels structurally amended via covalent attachment of surface-modified silica particles, Int. J. Biol. Macromol. 136 (2019) 1196–1208, doi:10.1016/j.ijbiomac.2019.06.184.
[79] J. Huang, Y. Liang, Z. Jia, J. Chen, L. Duan, W. Liu, F. Zhu, Q. Liang, W. Zhu, W. You, J. Xiong, D. Wang, Development of magnetic nanocomposite hydrogel with potential cartilage tissue engineering, ACS Omega 3 (2018) 6182–6189, doi:10.1021/acsomega.8b00291.
[80] A. Sionkowska, Molecular interactions in collagen and chitosan blends, Biomaterials 25 (2004) 795–801, doi:10.1016/S0142-9612(03)00595-7.
[81] A. Boecker, S.C. Daeschler, U. Kneser, L. Harhaus, Relevance and recent developments of chitosan in peripheral nerve surgery, Front. Cell. Neurosci. 13 (2019) 104, doi:10.3389/fncel.2019.00104.
[82] T.Y. Liu, S.H. Hu, T.Y. Liu, D.M. Liu, S.Y. Chen, Magnetic-sensitive behavior of intelligent ferrogels for controlled release of drug, Langmuir 22 (2006) 5974–5978, doi:10.1021/la060371e.
[83] H. Huang, S. Delikanli, H. Zeng, D.M. Ferkey, A. Pralle, Remote control of ion channels and neurons through magnetic-field heating of nanoparticles, Nat. Nanotechnol. 5 (2010) 602–606, doi:10.1038/nnano.2010.125.
[84] R. Chen, G. Romero, M.G. Christiansen, A. Mohr, P. Anikeeva, Wireless magnetothermal deep brain stimulation, Science 347 (2015) 1477–1480, doi:10.1126/science.1261821.